Local and remote causes of the equatorial Pacific cold sea surface temperature bias in the Kiel Climate Model

Article

Accepted Version

Local and remote causes of the equatorial Pacific cold sea surface temperature bias in the Kiel Climate Model

Yuming Zhang[a,b], Tobias Bayr[b], Mojib Latif[b,c], Zhaoyang Song[d,e*], Wonsun Park[f,g], Annika Reintges[h]

[a]South China Institute of Environmental Sciences, Ministry of Ecology and Environment, 510530 Guangzhou, China

[b] GEOMAR Helmholtz Centre for Ocean Research Kiel, 24105 Kiel, Germany

[c] Faculty of Mathematics and Natural Sciences, Christian-Albrechts-University of Kiel, 24105 Kiel, Germany

[d] School of Atmospheric Sciences, Sun Yat-sen University, and Key Laboratory of Tropical Atmosphere–Ocean System, Ministry of Education, Zhuhai, China

[e] Southern Marine Science and Engineering Guangdong Laboratory (Zhuhai), Zhuhai, China

[f] Center for Climate Physics, Institute for Basic Science (IBS), Busan, Republic of Korea

[g] Department of Climate System, Pusan National University, Busan, Republic of Korea

[h] National Centre for Atmospheric Science, University of Reading, Reading, UK

*Correspondence: Zhaoyang Song (songzhaoy@mail.sysu.edu.cn);

https://orcid.org/0000-0003-4105-8682

Abstract:

We investigate the origin of the equatorial Pacific cold sea surface temperature (SST) bias and its link to wind biases, local and remote, in the Kiel Climate Model (KCM). The cold bias is common in climate models participating in the 5th and 6th phases of the Coupled Model Intercomparison Project. In the coupled experiments with the KCM, the interannually varying NCEP/CFSR wind stress is prescribed over four spatial domains: globally, over the equatorial Pacific (EP), the northern Pacific (NP) and southern Pacific (SP). The corresponding EP SST bias is reduced by 100%, 52%,

Early Online Release: This preliminary version has been accepted for publication in *Journal of Climate*, may be fully cited, and has been assigned 10.1175/JCLI-D-22-0874.1. The final typeset copyedited article will replace the EOR at the above DOI when it is published.

12% and 23%, respectively. Thus, the EP SST bias is mainly attributed to the local wind bias, with small but not negligible contributions from the extratropical regions. Erroneous ocean circulation driven by overly strong winds cause the cold SST bias, while the surface-heat flux counteracts it. Extratropical Pacific SST biases contribute to the EP cold bias via the oceanic subtropical gyres, which is further enhanced by dynamical coupling in the equatorial region.

The origin of the wind biases is examined by forcing the atmospheric component of the KCM in a stand-alone mode with observed SSTs and simulated SSTs from the coupled experiments. Wind biases over the EP, NP and SP regions originate in the atmosphere model. The cold EP SST bias substantially enhances the wind biases over all three regions, while the NP and SP SST biases support local amplification of the wind bias. This study suggests that improving surface-wind stress, at and off the equator, is a key to improve mean-state equatorial Pacific SST in climate models.

Keywords: Cold equatorial Pacific SST bias, surface wind bias, tropical Pacific ocean-atmosphere coupling

1 Introduction

Ocean-atmosphere coupling plays a fundamental role for the mean state and variability in the tropical Pacific. Both dynamical coupling via surface winds, affecting the ocean circulation, and thermodynamic coupling via the surface-heat fluxes have a strong influence on the SST and upper ocean temperature (e.g., Lloyd et al. 2009, Bayr et al. 2021). Despite great progress over the recent years, most coupled general circulation models (CGCMs) still exhibit significant errors in the mean state in tropical Pacific sector and its interannual variability associated with the El Niño/Southern Oscillation (ENSO) (e.g., Bellenger et al. 2014; Wang et al. 2014, Planton et al., 2021; Guilyardi et al., 2020).

A long-standing problem in CGCMs is the cold equatorial Pacific (EP) SST bias

Accepted for publication in *Journal of Climate.* DOI 10.1175/JCLI-D-22-0874.1.

(hereafter cold bias), which manifests as an excessive and overly narrow cold tongue extending far west into the warm pool (Davey et al., 2002; Guilyardi et al., 2009; Guilyardi et al., 2020). The cold bias substantially disturbs the atmospheric mean state as well as the atmospheric response to SST anomalies, with far reaching consequences for the local and global climate (Bayr et al., 2018; 2019b). The double intertropical convergence zone (ITCZ) pattern is another notable bias shared by CGCMs, which exhibits excessive precipitation off the equator, insufficient precipitation along the equator and a zonally oriented rain band in the southern tropical Pacific (Mechoso, 1995; Lin, 2007). The equatorial precipitation deficit is tightly linked to the cold bias through the Bjerknes feedback in models participating in the Coupled Model Intercomparison Project phase 5 (CMIP5) (Li and Xie, 2014).

CGCMs with a cold bias also tend to exhibit erroneous ENSO dynamics and properties (Guilyardi et al. 2009). Along with the cold bias, a too westward-located rising branch of the Walker Circulation weakens the amplifying wind feedback and the damping heat-flux feedback, and hampers simulated ENSO dynamics due to error compensation (Bayr et al. 2019a; Bayr et al., 2020; Ding et al., 2020). Moreover, CGCMs with a reduced cold bias simulate the seasonal phase locking of ENSO and ENSO asymmetry more realistically (Wengel et al. 2018; Bayr et al., 2021).

Recent studies also suggest that the cold bias may also explain why current climate models are unable to simulate the observed SST cooling and strengthening of the Pacific Walker Circulation in the recent decades (Seager et al., 2019; 2022). Linked to the cold tongue bias, CMIP5 models generally exhibit higher relative humidity and lower wind speed, both of which contribute to a too high sensitivity of the SSTs in the region to rising greenhouses gases and hence, overwhelm the effect of upwelling (Seager et al., 2019). The cold bias also seems to introduce uncertainty to global warming projections of ENSO-amplitude change, as climate models with a small cold bias and realistic ENSO asymmetry agree on increasing ENSO amplitude under global warming (Cai et al., 2021), while there is still a large disagreement amongst all CMIP5 and CMIP6 models (Beobide-Arsuaga et al., 2021).

Further, the atmospheric teleconnections between the tropical Pacific and the

Accepted for publication in *Journal of Climate.* DOI 10.1175/JCLI-D-22-0874.1.

other tropical ocean basins as well as to the mid-latitudes may benefit by alleviating the cold bias (Alexander et al., 2002; Yeh et al. 2018; Timmermann et al. 2018). For example, in CMIP5 models the cold bias leads to a westward shift in the atmospheric response to ENSO over the North Pacific and significant underestimation of the ENSO-related precipitation anomalies over California (Bayr et al., 2019b). Therefore, addressing the cold bias is not only essential for improving tropical but also extratropical climate variability.

There are several systematic errors shared by the CGCMs, originating in the equatorial regions that may contribute to the cold bias (Vannière et al. 2013; Vannière et al. 2014). Lin (2007) found that excessive latent heat and insufficient shortwave radiation flux along with overly strong trade winds occur over the EP in stand-alone atmosphere-model simulations with prescribed observed SSTs. Stronger equatorial upwelling of cold water forced by too intense trade winds leads to the creation of a cold bias (Guilyardi et al. 2010). Both wind and SST biases are amplified by coupled ocean–atmosphere interaction related to the Bjerknes feedback (Li and Xie 2014; Mauritsen et al. 2012). Some studies trace the cold bias to deficiencies in the representation of atmospheric convection. A revised convection scheme can largely eliminate the cold bias and subsurface water-temperature biases, and the deficit in equatorial precipitation by strengthening negative shortwave flux–SST feedback and positive evaporation–SST feedback (Song and Zhang 2009). Other studies suggest that the cold bias is caused by too weak surface heating due to weak cloud responses to atmospheric ascent (Sun et al. 2003; Ferrett et al., 2018).

Regions off the equator can affect the EP SST through the atmospheric bridge in association with the atmospheric Rossby waves and the oceanic bridge through thermocline subduction (McCreary and Lu 1994; Liu and Yang 2003). Among these factors, easterly wind biases over both the equatorial and off-equatorial region play an important role in generating the cold bias (Burls et al., 2017). The subtropical cells, which consist of subtropical subduction, equatorward advection of cool subsurface water and upwelling at the equator, are largely driven by the wind stress (McCreary and Lu, 1994). Thus, wind biases over the off-equatorial region could affect the equatorial

Accepted for publication in *Journal of Climate.* DOI 10.1175/JCLI-D-22-0874.1.

SST through the subtropical gyres (Thomas and Fedorov, 2017). Some studies have supported this hypothesis, demonstrating that in CGCMs the east–west EP-SST gradient is tightly linked to the meridional cloud-albedo gradient via advection by the subtropical gyres (Burls and Fedorov 2014; Burls et al., 2017).

While biases in the atmosphere model may largely explain the cold bias, the ocean model also contributes. Overly strong subsurface mixing has been proposed to cause the cold bias (Moum et al. 2013). Underestimated biogeochemical attenuation of penetrative shortwave radiation may cause spurious cooling in the eastern EP (Murtugudde et al. 2002). In addition to thermodynamic processes, the simulated spatial SST distribution is very sensitive to ocean-heat transport (Zhang and Song 2010). Eddy-resolving ocean models improve the simulation of small-scale ocean processes to large extent and hence the simulation of tropical Pacific mean climate and its variability (Small et al., 2014).

So far, efforts to reduce the cold bias have generally focused on tuning parameters of convection schemes, albedo of low stratus clouds or vertical mixing schemes over the equatorial and off-equatorial Pacific (Gordan et al., 2000; Richards et al., 2009; Guilyardi et al. 2010; Burls et al., 2017; Bayr et al., 2018). Here we explore and quantify the influence of an improved atmospheric circulation on the cold bias in a CGCM. To what extent can improved equatorial and off-equatorial atmospheric surface forcing affect the cold bias and by which mechanism?

We perform a set of dedicated experiments with the Kiel Climate Model (KCM, Park et al. 2009) forced by reanalysis wind stress. The individual contributions of surface wind biases in different regions to the cold bias are assessed. Further, the response of the surface winds to a biased SST in different regions is investigated with stand-alone atmosphere-model experiments.

The paper is organized as follows: Section 2 describes the datasets, model, experimental setup and the methods used in this study. The results of the model simulations are presented in Section 3. In Section 3.1, the SST and wind biases and their relation are described in the KCM and in the CMIP5/CMIP6 models. The influence of the surface-wind biases over different regions on the cold bias is explored

Accepted for publication in *Journal of Climate.* DOI 10.1175/JCLI-D-22-0874.1.

in Section 3.2 with a set of coupled experiments. The mechanisms behind the cold bias are described in Section 3.3. The response of the surface winds to SST biases in different regions is investigated in Section 3.4 with a set of stand-alone atmosphere-model experiments. Summary and discussion are presented in Section 4.

2 Data, model and method

2.1 Observational and reanalysis datasets

To quantify the biases in the coupled and uncoupled experiments, the model results are compared to reanalysis data and where possible to observations. To obtain the mean-state SST biases, the monthly version of Hadley Centre Sea Ice and Sea Surface Temperature dataset (HadISST v1.1, Rayner et al. 2003) averaged over the period 1982-2017 is used. Zonal-mean upper-ocean temperature is compared against the average over 1975-2004 from the World Ocean Atlas 2018 (Boyer et al., 2018). The wind biases are mainly estimated by comparing the model data to the 10-m winds from the National Centers for Environmental Prediction Climate Forecast System Reanalysis (NCEP/CFSR, Saha et al. 2010) averaged over the period 1982-2017. Wind biases relative to ERA-Interim and ERA5 reanalyses are considered as well (Dee et al., 2011; Hersbach et al. 2018). Surface sensible and latent heat fluxes are taken from the Objectively Analyzed air-sea fluxes (OAFlux) dataset (Yu et al., 2008) averaged over the period 1983-2017. Net surface shortwave and longwave radiative flux and cloud cover are taken from the third-generation, high-resolution version of the International Satellite Cloud Climatology Project flux product (ISCCP-FH; Zhang and Rossow, 2022) available over the period 1983-2017. Interannually varying monthly NCEP/CSFR surface-wind stress spanning 1982-2017 is employed to force the coupled model. We choose the HadISST and the NCEP/CFSR to estimate the SST and wind biases, as the HadISST exhibit negligible differences relative to the Optimum Interpolation SST (not shown), to which the NCEP/CFSR wind stresses are strongly relaxed to.

2.2 Model and experimental setup

In this study, coupled and stand-alone atmosphere-model experiments are conducted with the KCM and its atmospheric component, respectively. The KCM is a

Accepted for publication in *Journal of Climate.* DOI 10.1175/JCLI-D-22-0874.1.

fully coupled atmosphere-ocean-sea ice general circulation model, which consists of the atmosphere model ECHAM5 (Roeckner et al., 2003) and the ocean-sea ice model NEMO (Madec, 2008). ECHAM5 is used with a T42 horizontal resolution (~2.8° × 2.8°) and with 19 vertical levels. The horizontal resolution of NEMO is approximately 2° (ORCA2 grid), with a meridional refinement of ~0.5° near the equator and 31 vertical levels.

We first consider a present-day control integration of the KCM (hereafter KCM_{CTR}). The KCM_{CTR} is initialized from the Levitus climatology and integrated for 110 years. Concentrations of greenhouse gases used in the KCM_{CTR} are representative of the mid 1980s. Specifically, the CO_2-concentration amounts to 348 ppm (parts per million), the CH_4-concentration to 1,650 ppb (parts per billion) and the N_2O-concentration to 306 ppb. The monthly output of the last 36-years is used for analysis. The HadISST considered is over the period of 1982-2017. Owing to different radiative forcings, the simulated global mean SST in the KCM_{CTR} tend to differ from the HadISST. To enable a fair comparison, we compute the relative SST bias by subtracting the area averaged SST over the tropical Pacific (20°S-20°N, 120°E-70°W). Studies suggest that the relative SSTs is depicts the relation between SSTs and tropical atmospheric convection better than the absolute SSTs (He et al., 2018; Izumo et al., 2019). The KCM, as many other coupled climate models, suffers from significant SST and 10-m wind biases over the tropical and extratropical Pacific (Figure 1). Figure 1a and Figure 1d depict the relative SST and the 10-m wind speed bias in the KCM_{CTR}, respectively, which both exhibit a banded structure in the zonal direction. Three regions, where cold SST biases coexist with positive wind-speed biases, are highlighted by the blue boxes in Figure 1. We define these regions as the northern Pacific (NP, 15°N-38°N, 130°E-130°W), equatorial Pacific (EP, 5°S-5°N, 130°E-100°W) and southern Pacific (SP, 35°S-15°S, 160°E-90°W).

Accepted for publication in *Journal of Climate.* DOI 10.1175/JCLI-D-22-0874.1.

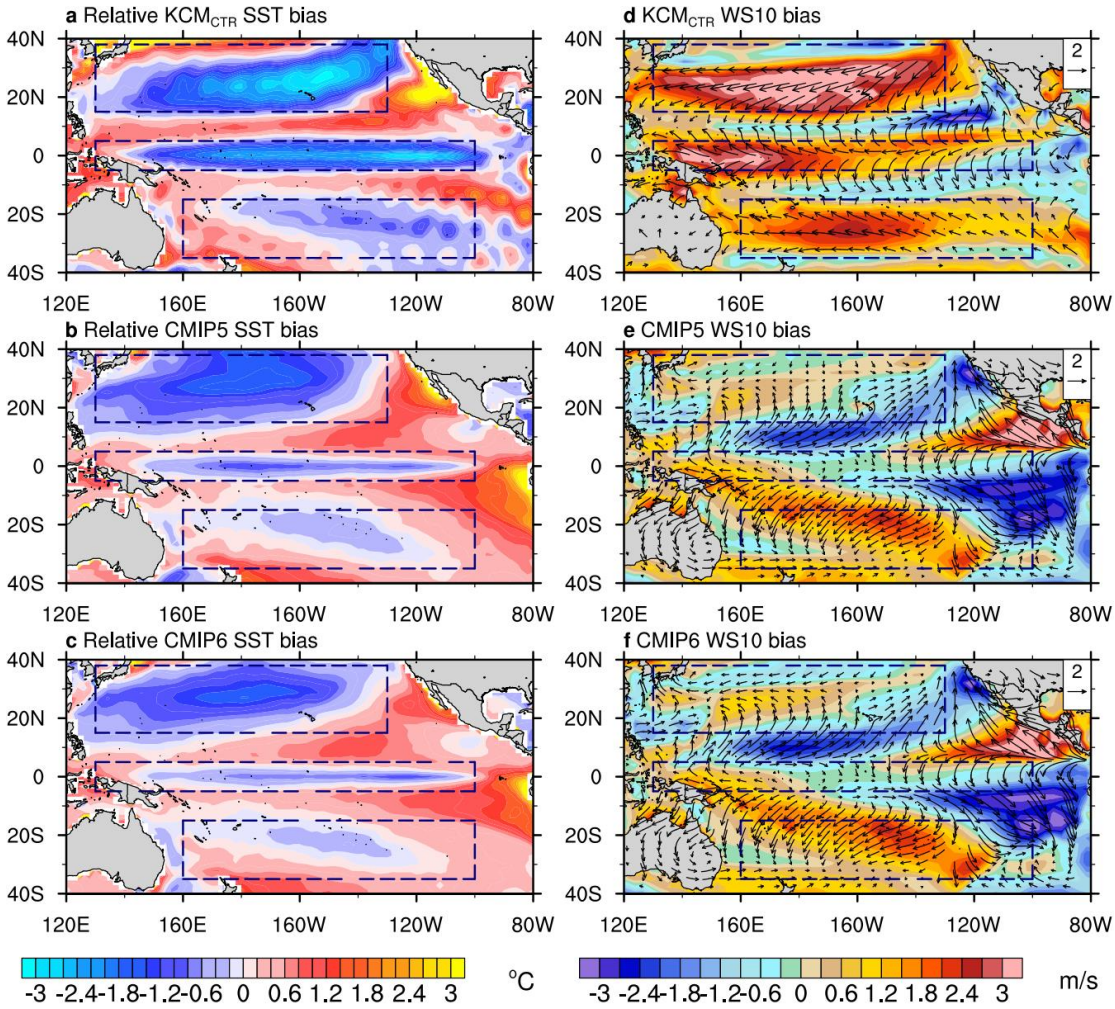

Figure 1. (a-c) Relative sea surface temperature (SST) bias (unit: °C) in KCM$_{CTR}$ (a), the CMIP5 (b) and the CMIP6 (c) multi-model mean relative to the HadISST v1.1 averaged over the period 1982-2017. The relative SST bias is computed by subtracting the area averaged SST over the tropical Pacific (20°S-20°N, 120°E-70°W). (d-e) 10-m winds (vectors, unit: m/s) and wind speed biases (shading, unit: m/s) in KCM$_{CTR}$ (d), the CMIP5 (e) and the CMIP6 (f) multi-model mean relative to the NCEP/CSFR reanalysis averaged over the period 1982-2017. Dashed boxes indicate the equatorial Pacific (EP, 5°S-5°N, 130°E-100°W), northern Pacific (NP, 15°N-38°N, 130°E-130°W) and southern Pacific (SP, 35°S-15°S, 160°E-90°W), respectively.

We performed a set of coupled experiments with the KCM and a set of stand-alone experiments with the ECHAM5 (Table 1). Four coupled sensitivity experiments have been conducted, in which the interannually varying NCEP/CSFR monthly wind stress is prescribed over the NP, EP, SP and globally (hereafter NP-Wind, EP-Wind, SP-Wind

Accepted for publication in *Journal of Climate*. DOI 10.1175/JCLI-D-22-0874.1.

and Global-Wind, respectively). In each sensitivity experiment, the wind-stress forcing, spanning 1982-2017, is repeated three times. The SST bias, especially over the equatorial Pacific, fully develops in the first two forcing cycles consistent with Vannière et al. (2014). The monthly output from the last forcing cycle is taken for analysis. We examine with this set of experiments the influence of realistic wind-stress forcing on the SST biases.

Table 1. Experimental setup for the coupled and stand-alone atmospheric experiments.

Model	Name	Forcing
KCM	KCM_{CTR}	N/A
	Global-Wind	NCEP/CSFR wind stress globally from 1982 to 2017
	NP-Wind	NCEP/CSFR wind stress over the Northern Pacific (15°-38°N, 130°E-130°W) from 1982 to 2017
	EP-Wind	NCEP/CSFR wind stress over the Equatorial Pacific (5°S-5°N, 130°E-100°W) from 1982 to 2017
	SP-Wind	NCEP/CSFR wind stress over the Southern Pacific (35°-15°S, 160°E-90°W) from 1982 to 2017
ECHAM5	$ECHAM5_{CTR}$	HadISST
	$ECHAM5_{Biased\text{-}NP\text{-}SST}$	KCM-CTR monthly cold SST bias in NP (15°-38°N, 130°E-130°W) + HadISST from 1982 to 2017
	$ECHAM5_{Biased\text{-}EP\text{-}SST}$	KCM-CTR monthly cold SST bias in EP (5°S-5°N, 130°E-100°W) + HadISST from 1982 to 2017
	$ECHAM5_{Biased\text{-}SP\text{-}SST}$	KCM-CTR monthly cold SST bias in SP (35°-15°S, 160°E-90°W) + HadISST from 1982 to 2017

The second set of experiments consists of an atmosphere-only control simulation (hereafter $ECHAM5_{CTR}$) and three uncoupled sensitivity experiments. In the $ECHAM5_{CTR}$, monthly SST and sea ice (HadISST) from 1982 is used as forcing during the initial three model years. Thereafter, the HadISST over the period 1983-2017 is applied. In the atmospheric sensitivity experiments, the HadISST forcing over the NP, EP and SP region is completely replaced by the biased SSTs from the KCM_{CTR} (hereafter $ECHAM5_{Biased\text{-}NP\text{-}SST}$, $ECHAM5_{Biased\text{-}EP\text{-}SST}$ and $ECHAM5_{Biased\text{-}SP\text{-}SST}$,

Accepted for publication in *Journal of Climate.* DOI 10.1175/JCLI-D-22-0874.1.

respectively). Such that the full impact of SST biases on the wind stress can be assessed. Each of these experiments is integrated for 38 years with the last 36 years used for analysis. Nonetheless, there are limitations of this approach. A spurious SST gradient is generated at the boundary where the biased SSTs are implemented, which may slightly affect the local response of wind stress to SST biases. Additionally, the temporal variability in the coupled model may be different from the observations, which creates some uncertainty in the simulated response of surface winds. We therefore define the response as annual changes in surface winds averaged over the last 36 years. This set of uncoupled experiments helps us to investigate the response of the surface winds to the cold SST biases in the NP, EP and SP regions separately.

2.3 Methods

A heat budget analysis over the upper ocean is applied to quantify the relative contributions of surface-heat flux and ocean dynamical heating processes to changes in the SST. Following DiNezio et al. (2009), the heat budget of the mixed layer can be expressed as,

$$\delta Q = Q_{\text{net}} - Q_{SWpen} + Q_{dyn} + Q_{residual} \quad (1)$$

Here Q_{net} and Q_{SWpen} represent net surface-heat flux and the amount of solar radiation transferred to the ocean at the bottom of the mixed layer, respectively. When the mixed-layer depth (MLD) is sufficiently large, Q_{SWpen} can be neglected.

The resolved oceanic heat transport Q_{dyn} can be written as

$$Q_{\text{dyn}} = Q_{\text{u}} + Q_v + Q_w. \quad (2)$$

Here Q_u, Q_v and Q_w are the zonal, meridional and vertical dynamical heating components, respectively. They are defined as,

$$Q_u = -\rho_0 c_p \int_{-H}^{0} u \frac{\partial T}{\partial x} dz, \quad (3)$$

$$Q_v = -\rho_0 c_p \int_{-H}^{0} v \frac{\partial T}{\partial y} dz, \quad (4)$$

$$Q_w = -\rho_0 c_p \int_{-H}^{0} w \frac{\partial T}{\partial z} dz, \quad (5)$$

where $\rho_0 c_p = 4.1 \times 10^6\ \text{J} \cdot \text{m}^{-3} \cdot \text{K}^{-1}$ is the product of the ocean density and the specific heat of seawater and H is the MLD.

Accepted for publication in *Journal of Climate.* DOI 10.1175/JCLI-D-22-0874.1.

$Q_{Residual}$ is the residual term which includes all processes that cannot be computed, such as mesoscale eddies, vertical and horizontal mixing, etc, as well as possible errors in other terms. Contributions from high-frequency processes are also included in this term. We evaluate the annual mean changes in the surface heat flux and ocean heat transport averaged over one forcing cycle as, i.e., 36 years, as the contributions to the SST biases. As the annual SST biases averaged in the last forcing cycle reach a quasi-steady state, the heating rate δQ is approximately equal to zero. Thus, the residual term $Q_{residual}$ can be estimated from the imbalance between the net surface-heat flux Q_{net} and the resolved oceanic heat transport Q_{dyn}.

A constant MLD of 50 m is chosen in the heat budget analysis, which corresponds to the average MLD in the equatorial Pacific. A 20 m shallower or deeper MLD would have negligible impact on the results. Further, this MLD is sufficiently large compared to the penetrative depth of shortwave radiation estimated using satellite ocean-colour data (Murtugudde et al. 2002).

3 Results

3.1 Equatorial and off-equatorial bias in the coupled experiments

Figure 1 shows the relative SST and absolute 10-m wind-speed biases in the Pacific with respect to HadISST and the NCEP/CFSR reanalysis, respectively, over the period 1980-2005 for the KCM_{CTR}, the multi-model mean of 26 CMIP5 and 33 CMIP6 models. A list of the CMIP5 and CMIP6 models considered in this study can be found in Figure 2 and we use here all CMIP models for which the required variables are available. In the $KCM_{CTR,}$ there are significant cold biases in the EP, and in the subtropical regions especially in the Northern Hemisphere (Figure 1a). The relative SST in the KCM_{CTR} is lower by 1.12 °C relative to HadISST averaged over the EP (5°S-5°N, 130°E-100°W). Large 10-m wind-speed biases, which can be largely attributed to the zonal wind component, go along with the SST biases over the aforementioned three regions (Figure 1d). Additionally, the KCM_{CTR} as well as the CMIP5 and CMIP6 models exhibit large warm SST biases along the Peruvian and Californian coast (Figure 1). These warm biases can be caused by erroneous meridional winds leading to reduced

Accepted for publication in *Journal of Climate.* DOI 10.1175/JCLI-D-22-0874.1.

upwelling (Harlaß et al., 2017) and/or underestimated formation of low-level stratus clouds (Mechoso et al. 1995). Corrected wind stress reduces the SST bias along the Californian coast but less clearly along the Peruvian coast (Figure 3). The physical mechanisms giving rise to the coastal warm SST biases, however, is beyond the scope of this study.

The SST and wind biases over these regions, especially over the EP, persist throughout the year with also seasonal variations (Figures S1 and S2). The entanglement between the annual mean biases and its seasonal cycle would lead to a very complex analysis and is beyond the scope of this study. We focus in the following on the annual-mean SST biases.

We calculate from the CMIP5 and CMIP6 historical simulations the biases over the period 1980 to 2005 (Taylor et al., 2012; Eyring et al., 2016). The cold SST and 10-m wind biases in CMIP5 and CMIP6 (Figure 1b-1f) somewhat resemble the banded pattern in the KCM_{CTR}, albeit they are slightly smaller - possibly due to bias compensation among different models (Figures S3-S6). Major differences between the KCM_{CTR} and the CMIP5 and CMIP6 models are observed in wind-speed biases, where the CMIP5 and CMIP6 models largely agree with each other, pointing towards different physical processes underlying the biases in the KCM_{CTR} and in the CMIP models. ERA-interim and ERA5 reanalyses are used to estimate 10-m wind biases in the KCM, the CMIP5 and CMIP6 models (Figure S7), which are of the same sign over most of the tropical Pacific.

Figure 2a (b) shows that there is a statistically significant relationship between the equatorial SST bias and the local surface wind speed (10-m zonal surface wind) with a correlation of 0.74 (0.71) considering models all together (KCM, the CMIP5 and CMIP6), suggesting an important role of dynamical atmosphere-ocean coupling in amplifying the cold tongue bias in the CMIP models (Li and Xie, 2014). We note that the cold tongue bias in the KCM_{CTR} is larger than that in most historical simulations by the CMIP models. This could be due to relatively low horizontal resolution and/or the tuning of convective parameters in the KCM_{CTR}. Additionally, there exists positive correlations between the equatorial zonal wind bias and the off-equatorial zonal wind

Accepted for publication in *Journal of Climate.* DOI 10.1175/JCLI-D-22-0874.1.

biases in the subtropical gyres. The CMIP5 models generally depict stronger equatorial linkages to the zonal winds in the subtropics than the CMIP6 models (Figures 2c and 2d). As shown by the KCM and all considered CMIP models, the correlation between the EP zonal wind bias and the NP zonal wind bias amounts to r=0.41 which is comparable to the correlation with its southern counterpart of r=0.44 (Figures 2c and 2d). Both correlation coefficients are significant at the 95% confidence level against the Pearson correlation coefficient. The individual influence of the zonal and meridional components is assessed through two complementary experiments (not shown). Their analysis shows that the influence of the wind biases on the EP SST bias is dominated by the zonal wind bias, the meridional wind bias appears as less crucial.

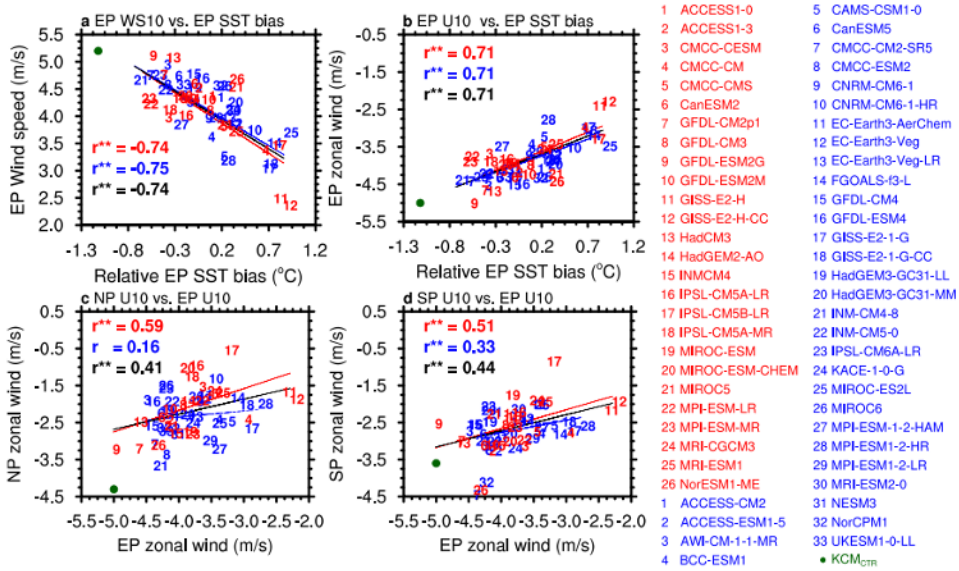

Figure 2. Relations between the relative sea surface temperature (SST) bias and 10-m winds in the KCM$_{CTR}$, CMIP5 and CMIP6 models. Scatter plot of (a) 10-m wind speed (unit: m/s) and (b) 10-m zonal wind (unit: m/s) over the equatorial Pacific (EP; 5°S-5°N, 130°E-100°W) versus local SST bias (unit: °C) for the CMIP5 and CMIP6 models. Scatter plot of 10-m zonal wind over the (c) NP and (d) SP versus 10-m zonal wind over the EP. Red and blue numbers represent the CMIP5 and CMIP6 models, respectively. The red, blue and black solid (dashed) lines indicate the significant (insignificant) linear regression for the CMIP5, CMIP6 and all CMIP models. The linear correlation coefficient (r) is given in the upper or lower right corner, with no, one or two stars indicating an insignificant correlation, a significant correlation at the 90%

Accepted for publication in *Journal of Climate*. DOI 10.1175/JCLI-D-22-0874.1.

or 95% confidence level using the Pearson correlation coefficient, respectively.

3.2 Response of SSTs to the surface winds in the coupled experiments

The above analysis suggests that the equatorial cold bias has a local origin involving dynamic coupling with the zonal wind, but also remote contributions from the northern and southern subtropical gyres. To verify this hypothesis, we perform sensitivity experiments with the KCM suffering from similar biases as that observed in many CMIP models.

In these sensitivity experiments, the KCM is forced by NCEP/CFSR reanalysis wind stress over different regions. Figure 3 depicts the SST responses relative to the KCM_{CTR} averaged over the period 1982-2017. When the interannually varying reanalysis wind stress is prescribed globally, the SSTs in the EP region warm by 1.14 °C corresponding to a complete reduction of the cold bias (Figures 3a and 3e). The differences between the Global-Wind and observations are not statistically significant (Figure S8). This suggests that the equatorial cold bias can be reduced by improving wind stress. When the reanalysis wind stress is only applied over the NP (Figure 3b), EP (Figure 3c) and SP region (Figure 3d), the cold bias in the equatorial Pacific is reduced by 0.14 °C (12%), 0.59 °C (52%) and 0.26 °C (23%), respectively (Figure 3e). Overall, the wind-stress biases over the three regions together explain 87% of the cold bias in the EP region assuming linearity of the response. We conclude that the biased wind stress over the EP (Figure 1d) is the major source of the equatorial cold bias in the KCM_{CTR} (Figure 3a and 3c). However, wind biases over the subtropical regions cannot be ignored when discussing the origin of the equatorial cold bias in the KCM_{CTR} (Figure 3b and 3d). The wind biases in the SP region exhibit a stronger influence on the equatorial cold bias relative to that in the NP region.

Accepted for publication in *Journal of Climate.* DOI 10.1175/JCLI-D-22-0874.1.

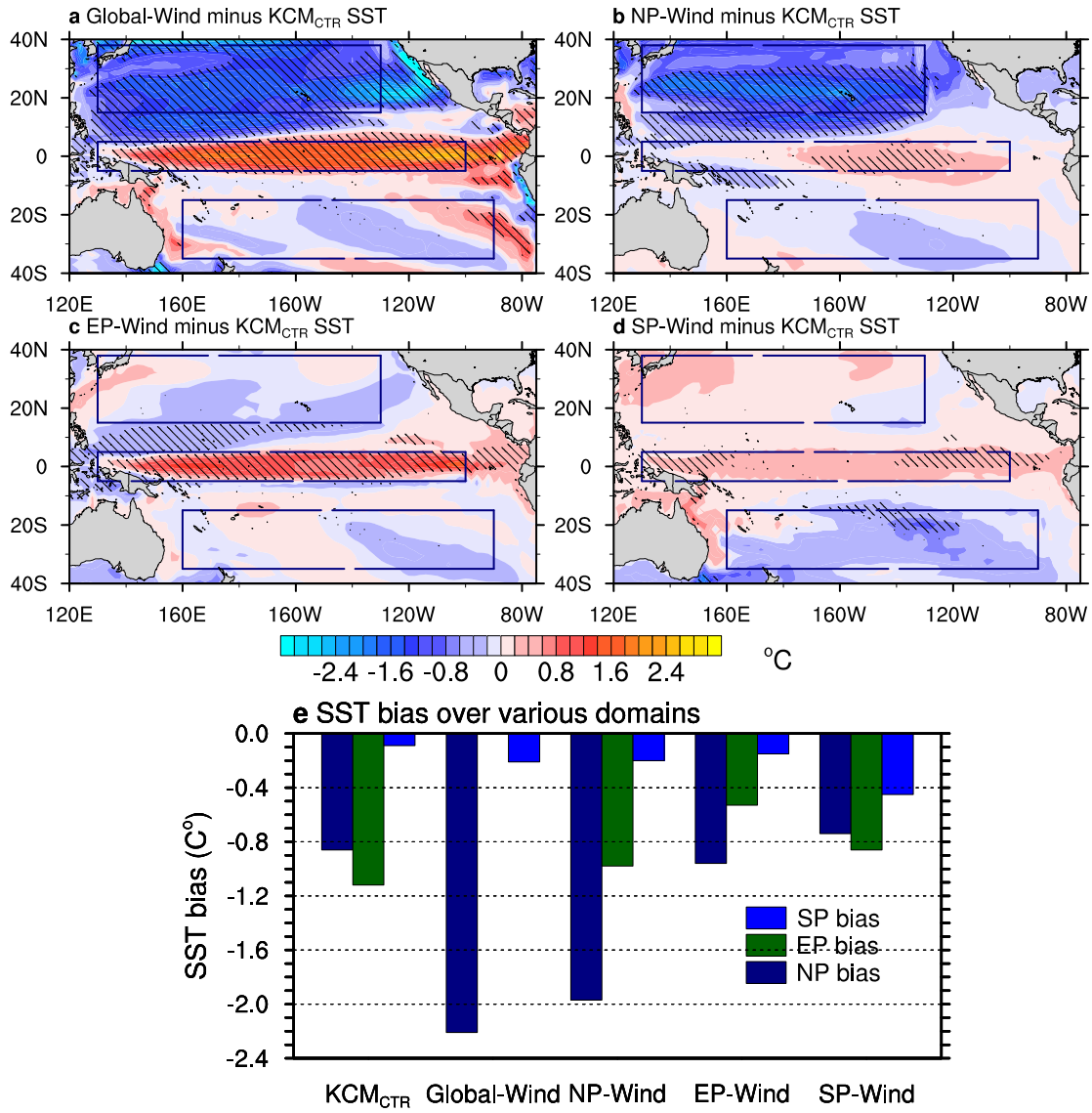

Figure 3. Sea surface temperature (SST) responses (unit: °C) in (a) Global-Wind, (b) NP-Wind, (c) EP-Wind and (d) SP-Wind relative to KCM_{CTR} averaged over the period 1982-2017. Hatching indicates that the differences are significant at the 95% confidence level using Student's t-test. (e) SST bias over various domains in KCM_{CTR} and four sensitivity experiments with respect to the HadISST v1.1 averaged over the period of 1982-2017.

Vertical sections of the zonally averaged upper-ocean temperatures and velocities averaged over 130°E-100°W from the KCM_{CTR} are shown in Figure 4a. The vertical velocities have been multiplied by 10^4 for better visibility. Pronounced Ekman cells, forced by the easterly wind stress at the equator, exist in both hemispheres, with

Accepted for publication in *Journal of Climate*. DOI 10.1175/JCLI-D-22-0874.1.

upwelling at the equator and divergent meridional velocities approximately in the upper 50 m giving rise to the minimum in the upper-ocean temperatures at the equator. Subsurface subtropical waters in the KCM_{CTR} suffer from marked cold biases, especially between 10°S and 20°S in the Southern Hemisphere (Figure 4b). The cold subsurface biases, connecting the subtropics with the equatorial upwelling, suggest that the equatorial cold bias in the KCM_{CTR} partly originates in the subtropics. Figures 4c-g depict the temperature and current responses in the sensitivity experiments relative to the KCM_{CTR}. The temperatures in the upper 80 m of the EP become warmer in all experiments, with the exception of the EP-Wind in which the warming only extends down to about 60 m. Warming in the EP is strongest at the surface in the Global-Wind and EP-Wind (Figure 4c and 4e). The oceanic current changes suggest that the warming in the top 80 m (Global-Wind) and top 60 m (EP-Wind) is linked to the weakening of the Ekman cells (Tropical Cells), which is associated with a reduced upwelling of cold subsurface waters to the surface. In the NP-Wind and SP-Wind, the warming in the equatorial region is much weaker and uniform over the upper 80 m, and is suggested to mainly result from the significantly reduced cold subsurface biases around 15°N (Figure 4d) and 15°S (Figure 4f). As shown in the Global-Wind and NP-Wind, correcting the wind stress in the NP region tend to amplify the local SST bias in NP, which is mainly attributed to increased equatorward horizontal transport of cold water and locally strengthened upwelling (Figure 4c and 4d). The subsurface cold bias in the Southern Hemisphere subtropics slightly intensifies in the NP-Wind, which may explain the smaller equatorial warming compared to the SP-Wind (Figure 4g).

Accepted for publication in *Journal of Climate.* DOI 10.1175/JCLI-D-22-0874.1.

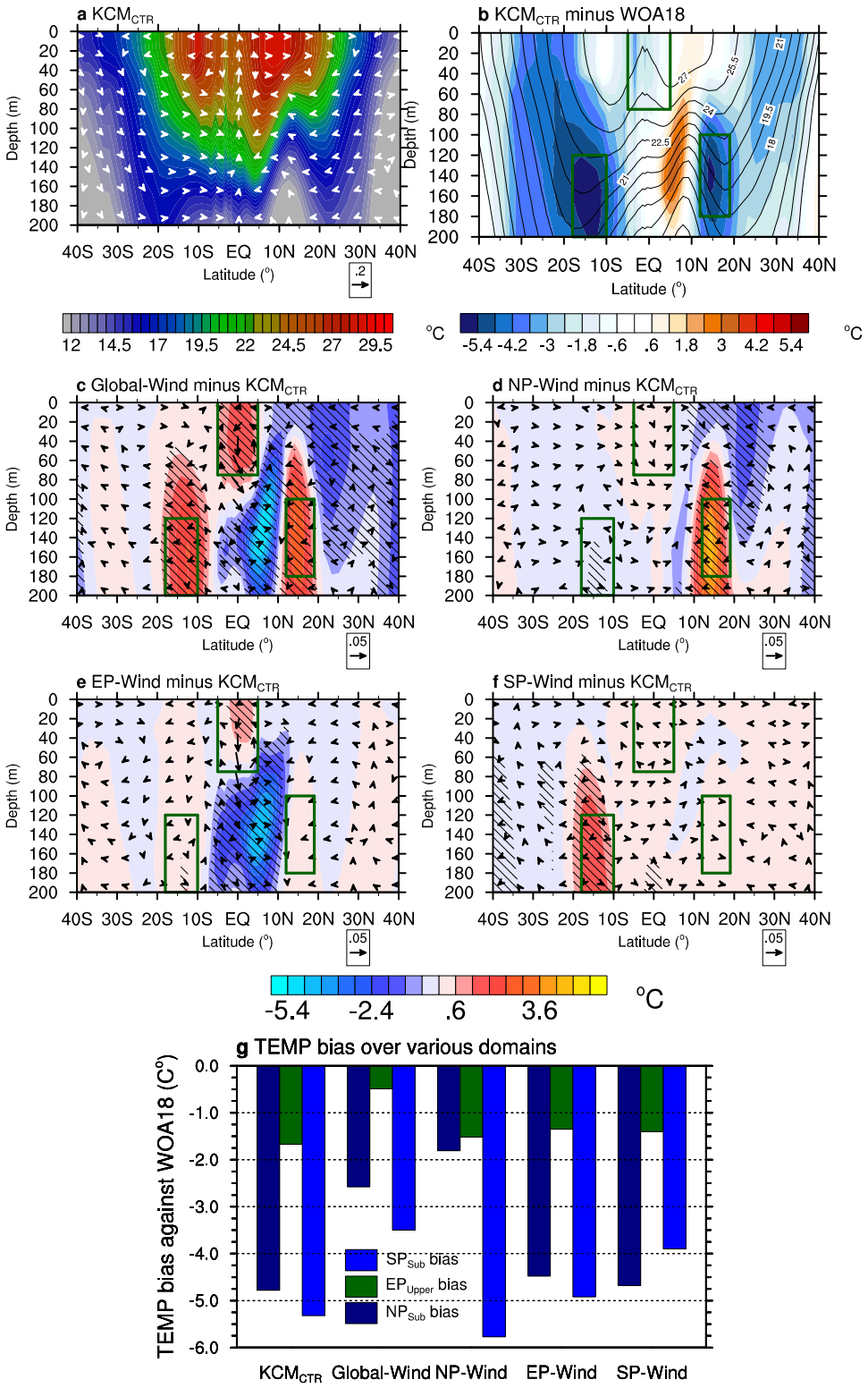

Figure 4. (a) The vertical profile of the zonal mean ocean temperature (shading, unit: °C) and velocities (vectors, unit: m/s) over 130°E and 100°W in KCM_{CTR}. The vertical current is multiplied by 10,000 for better visuality. (b) The vertical profile of bias (shading) in the zonal mean ocean temperature over 130°E and 100°W in KCM_{CTR}

Accepted for publication in *Journal of Climate.* DOI 10.1175/JCLI-D-22-0874.1.

with respect to the World Ocean Atlas 2018 (WOA18). Contours show the zonal mean temperature for the WOA18. Green boxes indicate the subsurface in the northern Pacific (NP_{Sub}, 12°N-19°N, 130°E-100°W, 100-180 m), upper layers in the equatorial Pacific (EP_{Upper}, 5°S-5°N, 130°E-100°W, 0-80 m) and the subsurface in the southern Pacific (SP_{Sub}, 10°S-18°S, 130°E-100°W, 120-200 m). Responses of ocean temperature (shading, unit: °C) and current (vectors, unit: m/s) in (c) Global-Wind, (d) NP-Wind, (e) EP-Wind and (f) SP-Wind relative to KCM_{CTR} over the period 1982-2017. Hatching indicates that the differences are significant at the 95% confidence level using Student's t-test. (g) Temperature biases over the three domains (as shown by the green boxes in Figure 4b) in KCM_{CTR} and four sensitivity experiments with respect to the WOA18.

To obtain more insight into the ocean-circulation changes, we calculate the wind-stress curl (Figure 5) and the barotropic streamfunction (Figure 6) in the different experiments, where the climatologies of the KCM_{CTR} are shown in Figures 5a and 6a. Differences of wind stress and wind-stress curl in the coupled sensitivity experiments are shown in Figure 5b-5e, which is a forcing by definition of the experimental set-up. In the off-equatorial region between 10°N and 25°N, enhanced equatorward oceanic mass transport is driven by the negative changes wind stress curl in the Global-Wind (Figure 5b). Similarly, enhanced yet weaker equatorward mass transport is forced in the South Pacific counterpart (Figure 5b). Additionally, weakened subtropical gyres driven by local wind forcing transports reduced warm water from the tropics to the central areas of the NP and SP basin in the Global-Wind, as indicated by the decreased meridional gradient in the barotropic streamfunction (Figure 6b), thereby contributing to the pronounced cooling in the subtropical Pacific, especially in the Northern Hemisphere (Figure 3). Near the equator between 5°S and 10°N, equatorial currents are weakened owing to the direct Ekman transport driven by substantially reduced meridional winds in addition to the positive wind stress curl (Figure 5b). As a result, reduced cold-water is exported from the cold tongue into the warm pool (Figure 6b), thereby warming the SSTs in the EP. The oceanic circulation changes in the NP-Wind and SP-Wind approximately depict the response in the Global Wind in the North and

Accepted for publication in *Journal of Climate.* DOI 10.1175/JCLI-D-22-0874.1.

South Pacific, respectively (Figures 5c and 5e, Figures 6c and 6e). Notably, in the off-equatorial region biases in surface winds and wind-stress curl also reduce in the EP-Wind, especially around 15°N & 15°S, indicating remote atmospheric responses to the alleviated equatorial SST bias (Figure 5d).

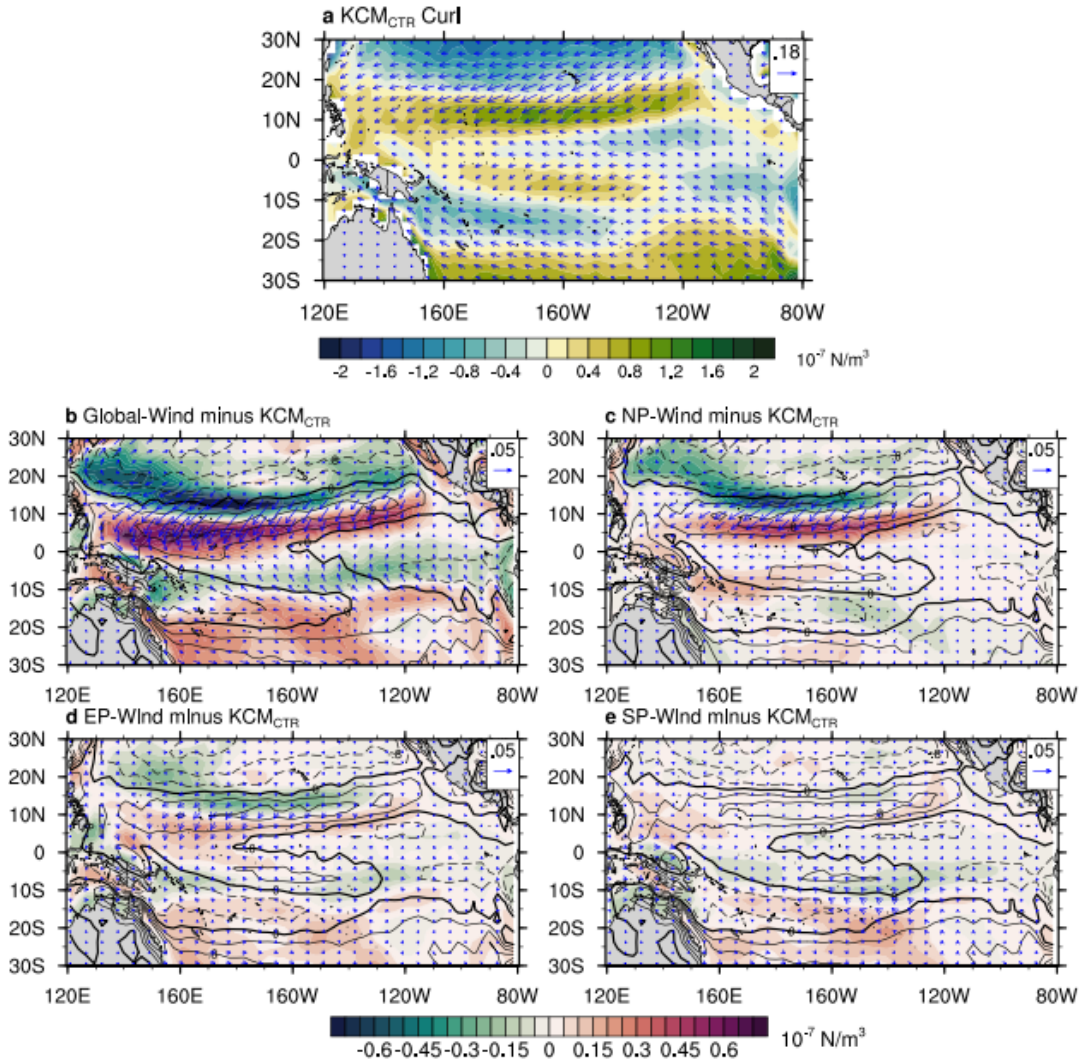

Figure 5. (a) Climatological mean wind stress (blue vectors, unit: N/m^2) and wind stress curl (shading unit: N/m^3) in KCM$_{CTR}$. Difference between prescribed wind stress (vectors) and wind stress curl (shading) in (c) Global-Wind, (d) NP-Wind, (e) EP-Wind and (f) SP-Wind experiments and simulated wind stress and wind stress curl in KCM$_{CTR}$ for the period 1982-2017. Contours in Figures 5b-5e show the climatological mean wind stress curl for (b) Global-Wind, (c) NP-Wind, (d) EP-Wind and (e) SP-Wind. The contour interval is 0.4×10^{-7} N/m^2.

Accepted for publication in *Journal of Climate*. DOI 10.1175/JCLI-D-22-0874.1.

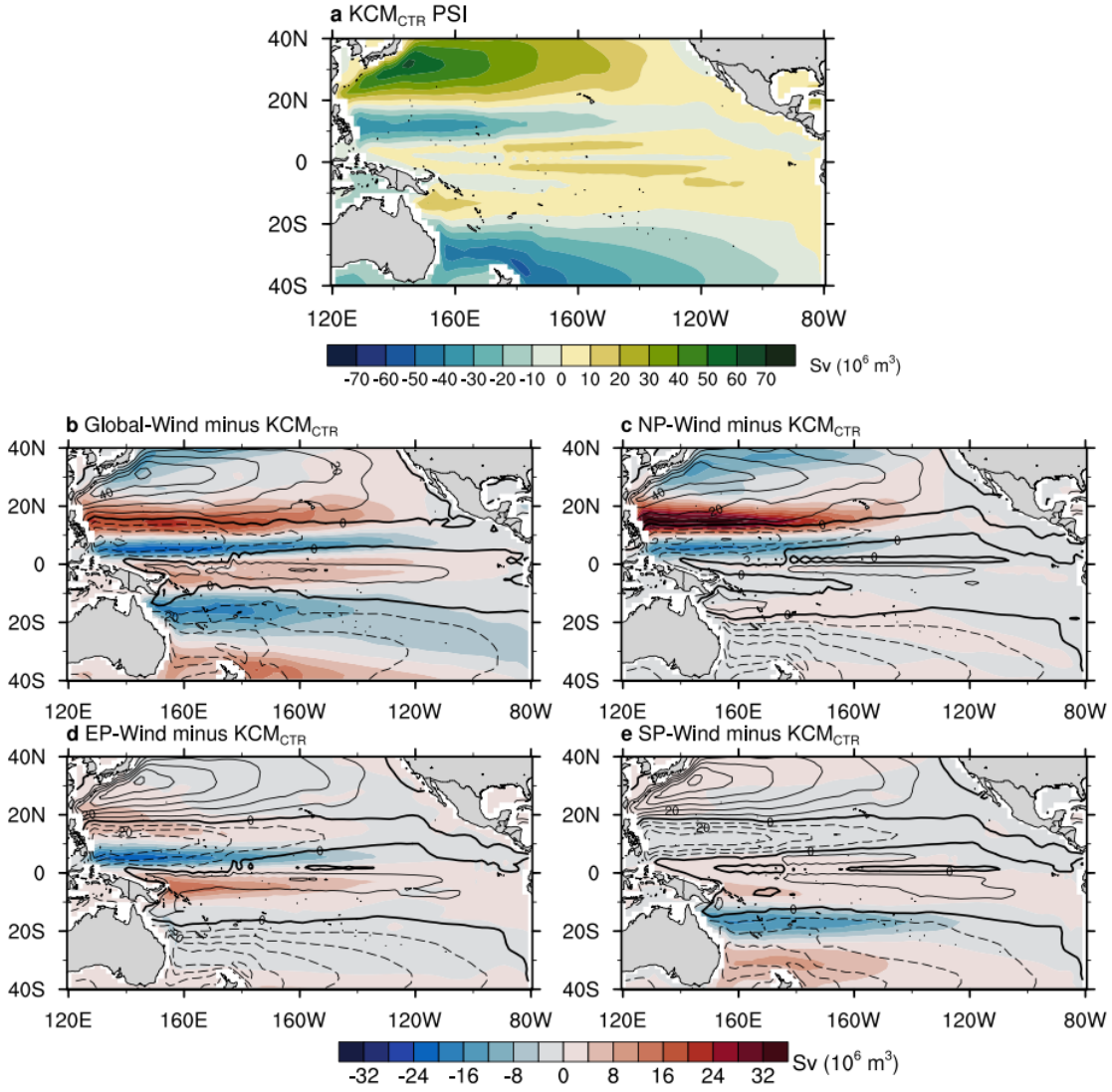

Figure 6. (a) Climatological mean barotropic streamfunction (PSI, unit: Sv, 1 Sv ≡ $10^6 m^3/s$) in KCM$_{CTR}$. In the meridional direction (from south to north), the increasing (decreasing) streamfunction stands for eastward (westward) volume transport. Responses of barotropic streamfunction (unit: Sv) in (b) Global-Wind, (c) NP-Wind, (d) EP-Wind and (e) SP-Wind experiments in relative to KCM$_{CTR}$ for the period 1982-2017. The contours in Figures 8b-8e show the climatological mean PSI for Global-Wind (b), NP-Wind (c), EP-Wind (d) and SP-Wind (e), respectively. The contour interval is 10 Sv.

3.3 Mixed layer heat budget in the coupled experiments

In this section, we quantify the contributions of ocean dynamical processes and

Accepted for publication in *Journal of Climate*. DOI 10.1175/JCLI-D-22-0874.1.

surface-heat flux to the SST responses in the sensitivity experiments with the KCM. Figure 7a depicts the time-averaged ocean dynamical heating (colour shading) and the horizontal ocean currents (vectors) averaged over the upper 50 m in the KCM_{CTR}. The ocean dynamics tend to cool the SST in the EP and to warm the off-equatorial Pacific in the KCM_{CTR}. Specifically, the zonal, meridional and vertical components of the ocean dynamical heating (Figures S9a, S9b and S10a) each contribute to the cooling in the EP, where the zonal component is largest at the equator, the meridional component just off the equator and the vertical component in the very east. Figures 7b-e depict the responses of the ocean dynamical heating and the horizontal ocean currents in the sensitivity experiments. The cooling effect by the ocean dynamics in the EP decreases in the four sensitivity experiments, thereby supporting SST warming relative to the KCM_{CTR} (Figure 3). The dynamical cooling averaged over the EP weakens by 42.5 W/m^2, 6.8 W/m^2, 27.8 W/m^2 and 5.8 W/m^2 in the Global-Wind, NP-Wind, EP-Wind and SP-Wind, respectively (Figure 8). The response of the ocean dynamical heating in the EP-Wind is 65% of that in the Global-Wind, which is comparable to the ratio (52%) of the reduced SST bias in the EP-Wind (0.59°C) and Global-Wind (1.14°C). Consistently, the responses of the ocean dynamical heating in the NP-Wind and SP-Wind are much weaker relative to the EP-Wind (Figure 7c and 7e). In terms of individual contributions, the zonal and meridional components of the ocean dynamical heating are comparable in magnitude and much larger than the vertical component (Figure 8). The response of the zonal dynamical heating component is strongest west of the dateline (Figures S9c, S9e, S9g and S9i), while that of the meridional component is more zonally uniform in the EP with a minimum at the equator (Figures S9d, S9f, S9h and S9j). The vertical ocean dynamical heating component only contributes close to the South American coast and in the eastern EP, and is relatively noisy (Figure S10).

Accepted for publication in *Journal of Climate.* DOI 10.1175/JCLI-D-22-0874.1.

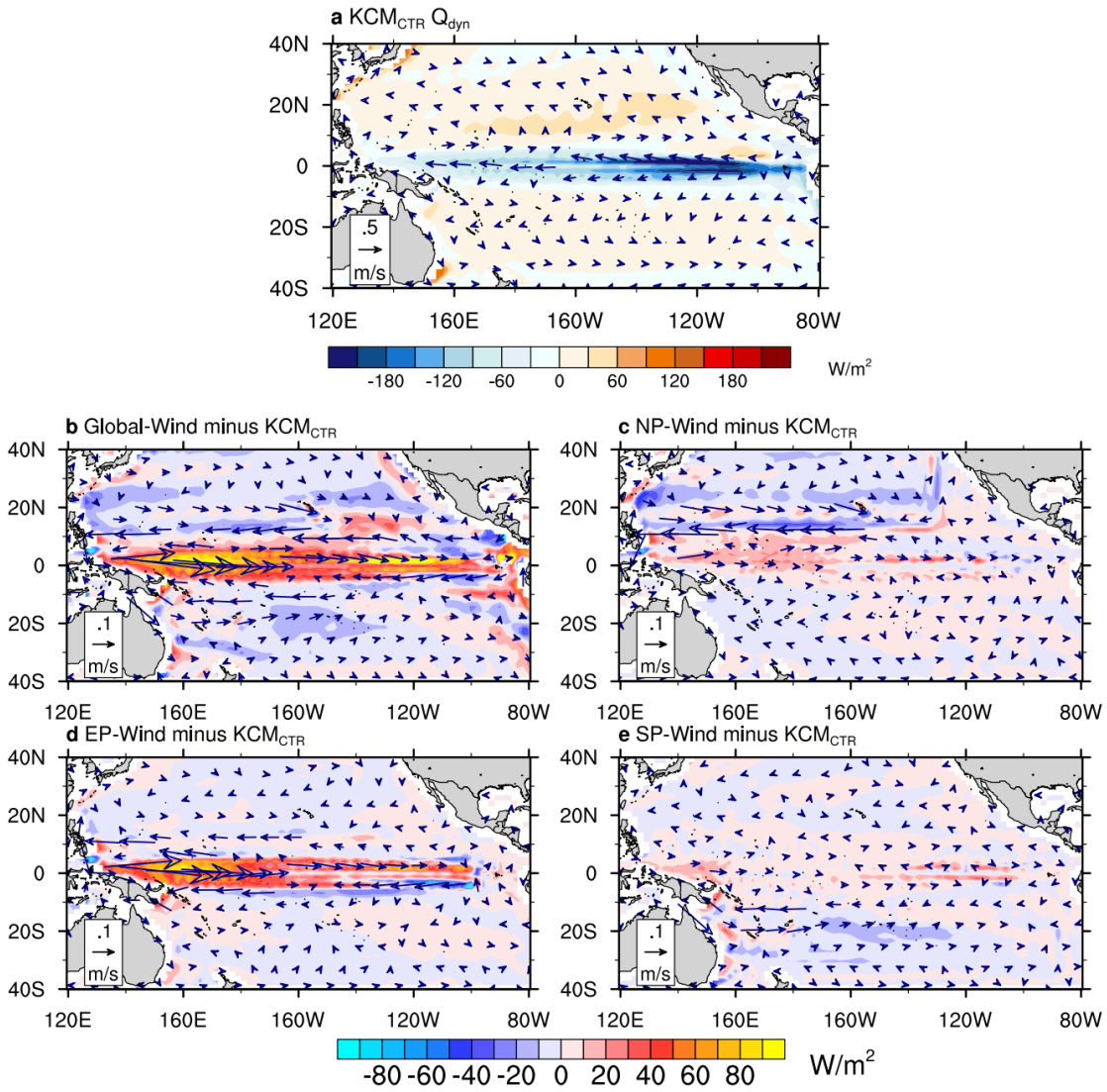

Figure 7. (a) Climatological mean ocean dynamical heating (shading, unit: W/m^2) and ocean horizontal current (vectors, unit: m/s) averaged in the upper 50-m in KCM$_{CTR}$. Responses of ocean dynamical heating (shading, unit: W/m^2) and ocean horizontal current (vectors, unit: m/s) in (b) Global-Wind, (c) NP-Wind, (d) EP-Wind and (e) SP-Wind relative to KCM$_{CTR}$ averaged over the period 1982-2017.

Accepted for publication in *Journal of Climate*. DOI 10.1175/JCLI-D-22-0874.1.

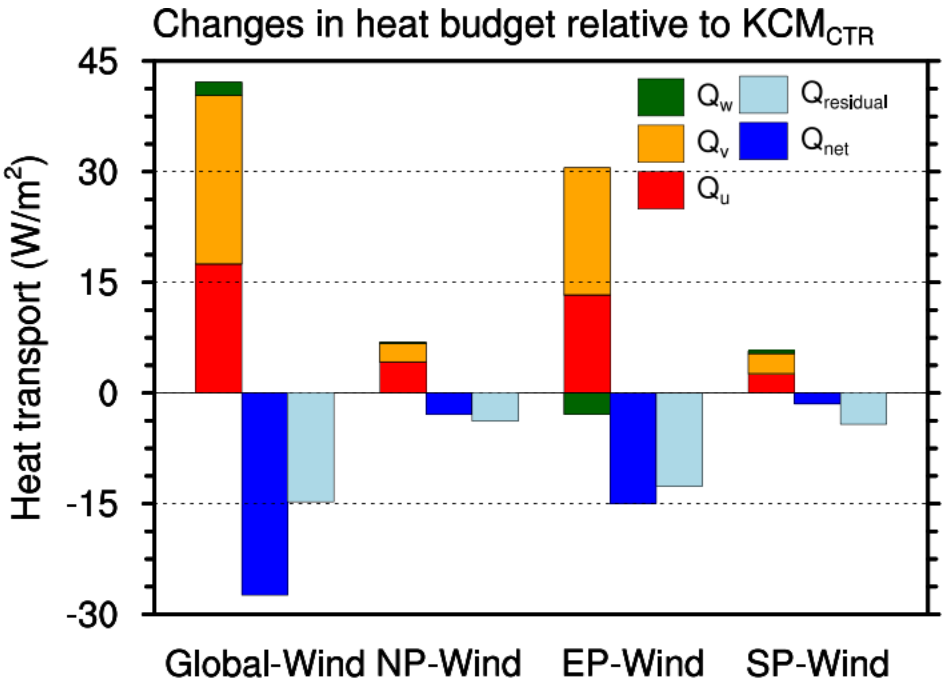

Figure 8. Responses of heat budget in the mixed layer over the equatorial Pacific (EP as defined in Figure 1) in the coupled sensitivity experiments relative to KCM$_{CTR}$. Q_u, Q_v and Q_w are the zonal, meridional and vertical dynamical heating components. Q_{net} represents net surface heat flux. $Q_{residual}$ is a residual term, which includes all processes that cannot be calculated with monthly output, as well as the possible errors in the other terms.

The changes in the zonal and meridional ocean dynamical heating components can be mainly attributed to the eastward and equatorward responses of the horizontal upper-ocean currents (Figure S9c-S9j). The eastward change in the zonal currents reduces the cold-water transport from the cold tongue towards the western Pacific warm pool, while the equatorward response of the meridional currents reduce the export of warm-water to the off-equatorial region. We note that the response of the vertical dynamical heating in the EP-Wind is small but negative (Figure 8), which represents a cooling influence on the SST, especially in the cold tongue region (Figure S10d). This cooling effect is linked to the stronger vertical temperature stratification overriding the effect of the weaker upwelling (Figure 4e). Unresolved oceanic processes as included by the residual term play an important role in damping SST biases (Figure 8). It is noted

Accepted for publication in *Journal of Climate*. DOI 10.1175/JCLI-D-22-0874.1.

that the actual mixed layer in the equatorial Pacific is deeper than 50 m in the west and shallower in the east. A constant MLD used in the heat budget analysis may thus create some uncertainty in the heat budget analysis, which is partly represented by the residual term.

Next, we examine the net surface-heat flux (Q_{net}) and cloud-cover responses in the coupled experiments. Figure 9a and Figure 10a present the long-term averages of Q_{net} and cloud cover simulated in the KCM_{CTR}. Strong positive (downward) Q_{net} associated with relatively low cloudiness occurs in the EP. Compared to the OAFlux observations, excessive downward Q_{net}, especially associated with too large surface solar radiation (not shown), is linked to a reduced cloud cover over this region (Figure 9b and 10b). This suggests that the biased Q_{net} and cloud cover in the KCM_{CTR} can be attributed to the compensation of the cold SST bias by the cloud-radiative effect. The responses of Q_{net} and cloud cover in the coupled sensitivity experiments are shown in Figure 9c-9f and Figures 10c-10f. Downward Q_{net} is reduced over the EP and increases over the subtropics (Figure 9c). This is accompanied by cloud-cover changes of opposite signs (Figure 10c), suggesting that the thermodynamic coupling counteracts the SST biases over the tropical Pacific. Therefore, prescribed surface-wind stress not only reduces SST biases, but also alleviates erroneous surface-heat fluxes and cloud clover. The largest changes in Q_{net} and cloud cover are observed over the western EP in the KCM_{CTR}, as well as in the NP-Wind (Figure 9d and Figure 10d), EP-Wind (Figure 9e and Figure 10e) and SP-Wind (Figure 9f and Figure 10f).

Accepted for publication in *Journal of Climate.* DOI 10.1175/JCLI-D-22-0874.1.

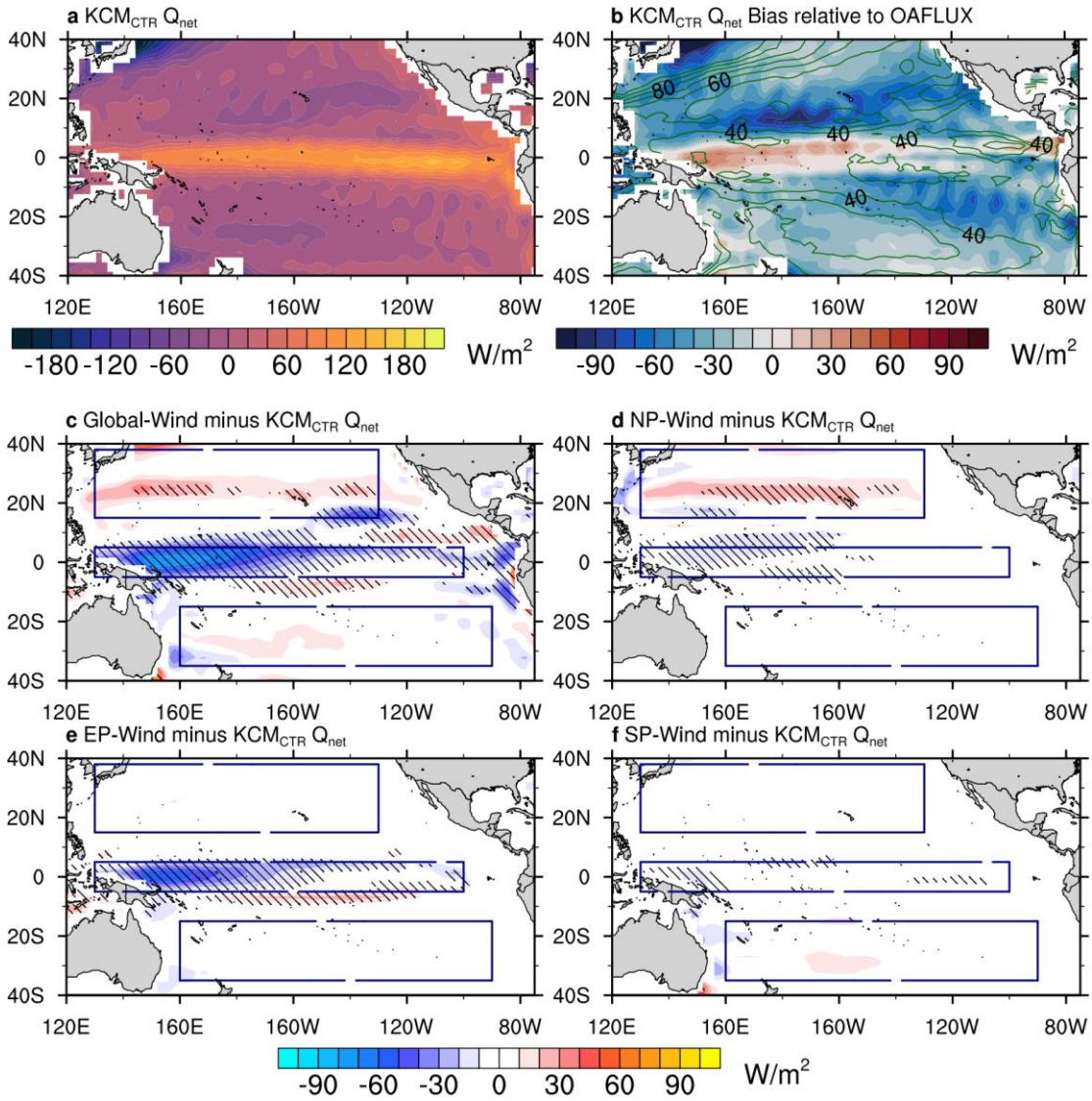

Figure 9. (a) Climatological mean net surface heat flux (Q_{net}, unit: W/m^2) in KCM$_{CTR}$. (b) Q_{net} bias relative to the OAFLUX averaged over the period of 1983-2017. Green contours indicate the uncertainty of Q$_{net}$ biases, defined as one standard deviation of monthly biases. Response of Q_{net} in (c) Global-Wind, (d) NP-Wind, (e) EP-Wind and (f) SP-Wind relative to KCM$_{CTR}$ averaged over the period of 1983-2017. Hatching indicates that the differences are significant at the 95% confidence level using Student's t-test.

Accepted for publication in *Journal of Climate*. DOI 10.1175/JCLI-D-22-0874.1.

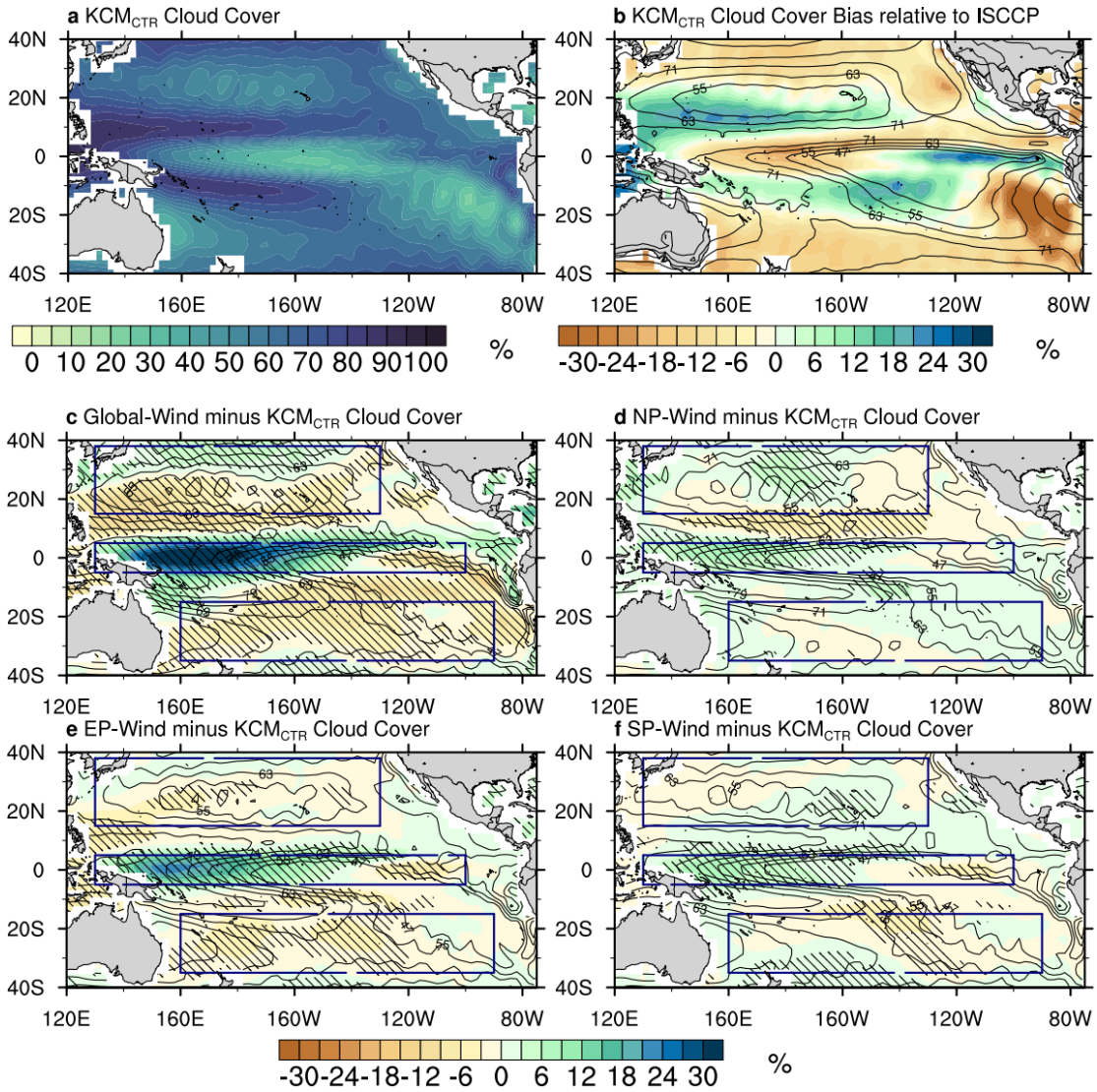

Figure 10. As in Figure 9, but here for the cloud cover (unit: %). Contours in Figures 10b-10f show the climatological mean wind stress curl for (b) the ISCCP, (c) Global-Wind, (d) NP-Wind, (e) EP-Wind and (f) SP-Wind. The contour interval is 8%.

3.4 Origin of wind bias

The question that still remains is the origin of the biased surface winds and their interaction with the SST. To address this question, we conducted a set of stand-alone experiments with the atmospheric component of the KCM, the ECHAM5 atmospheric general circulation model (AGCM).

Figure 11a shows near-surface (10-m) wind speed in the ECHAM5$_{CTR}$ forced by HadISST. There is a pronounced wind-speed bias relative to the NCEP/CFSR reanalysis that is mainly caused by too strong easterlies over the central equatorial, northern and

Accepted for publication in *Journal of Climate*. DOI 10.1175/JCLI-D-22-0874.1.

southern subtropical Pacific (Figure 11b). In contrast to ECHAM5$_{CTR}$, wind speed biases are even stronger over the eastern EP, central subtropical NP and SP in KCM$_{CTR}$ (Figure 1d). Differences in the pattern and intensity of wind biases between ECHAM5$_{CTR}$ and KCM$_{CTR}$ arise mainly from the ocean-atmosphere coupling.

In the ECHAM5$_{CTR}$, the wind bias averaged over the NP is 1.39 m/s and comparable to the bias of 1.70 m/s in the KCM$_{CTR}$ (Figure 12). On the other hand, the wind-speed bias over the EP and SP is smaller in the EHCAM5$_{CTR}$ than that in the KCM$_{CTR}$ (Figure 12). When the biased SST simulated in the KCM$_{CTR}$ is specified over the NP, the local wind-speed bias increases over the eastern subtropical NP and remains basically unchanged over the EP and SP (Figure 11c and Figure 12). In the ECHAM5$_{Biased\text{-}EP\text{-}SST}$, the surface winds over several regions, i.e., western equatorial Pacific, central and eastern subtropical NP and eastern subtropical SP, intensify in response to the too cold equatorial SSTs (Figure 11d). The averaged 10-m wind-speed bias over the NP, EP and SP regions strengthens to 1.75 m/s, 1.12 m/s and 1.22 m/s, respectively, which is comparable to that in the KCM$_{CTR}$ (Figure 12). This indicates an important role of the EP-SST bias for changing the local and subtropical wind biases from the pattern in ECHAM5$_{CTR}$ towards that in the KCM$_{CTR}$. Similar to the influence of the SST bias in the NP region, the biased SST in the SP region slightly strengthens the local bias over the central subtropical SP, with little impact over the NP and EP (Figure 11e, Figure 12).

Accepted for publication in *Journal of Climate.* DOI 10.1175/JCLI-D-22-0874.1.

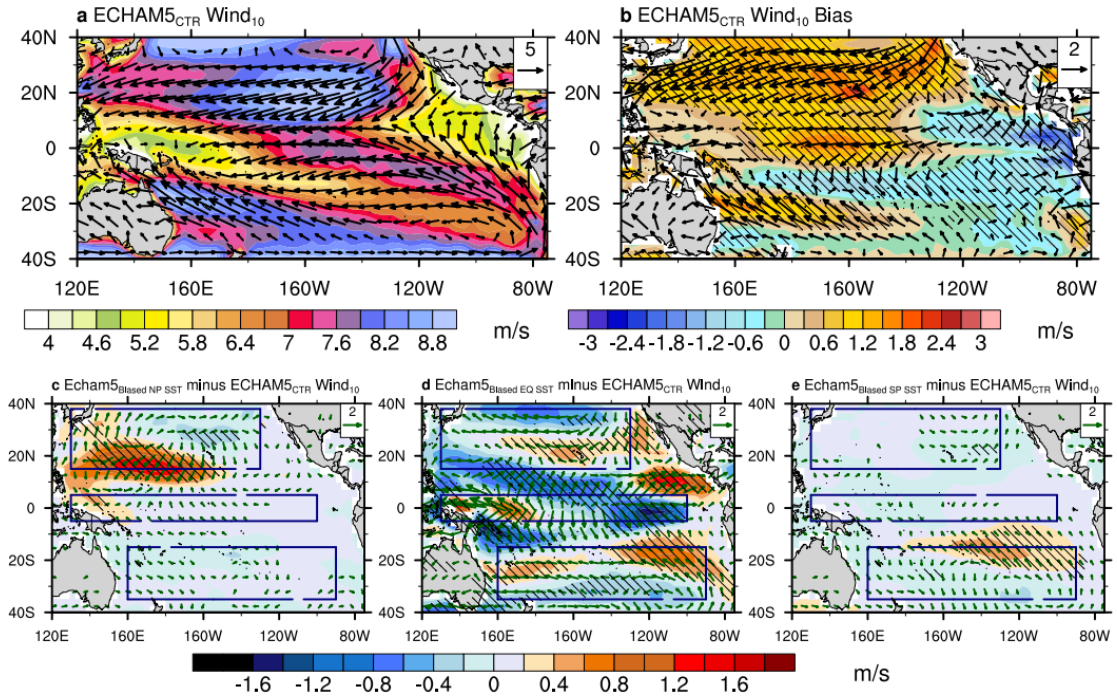

Figure 11. 10-m winds (vectors, unit: m/s) and wind speed (shading, unit: m/s) in (a) ECHAM5$_{CTR}$ spanning from 1982-2017. (b) Biases in 10-m winds and wind speed relative to the NCEP/CFSR reanalysis averaged over the period 1982-2017, respectively. Differences in 10-m winds and wind speed in (c) ECHAM5$_{Biased\text{-}NP\text{-}SST}$, (d) ECHAM5$_{Biased\text{-}EP\text{-}SST}$ and (e) ECHAM5$_{Biased\text{-}SP\text{-}SST}$ relative to ECHAM5$_{CTR}$. Hatching indicates the differences are statistically significant at the 95% confidence level using Student's t test.

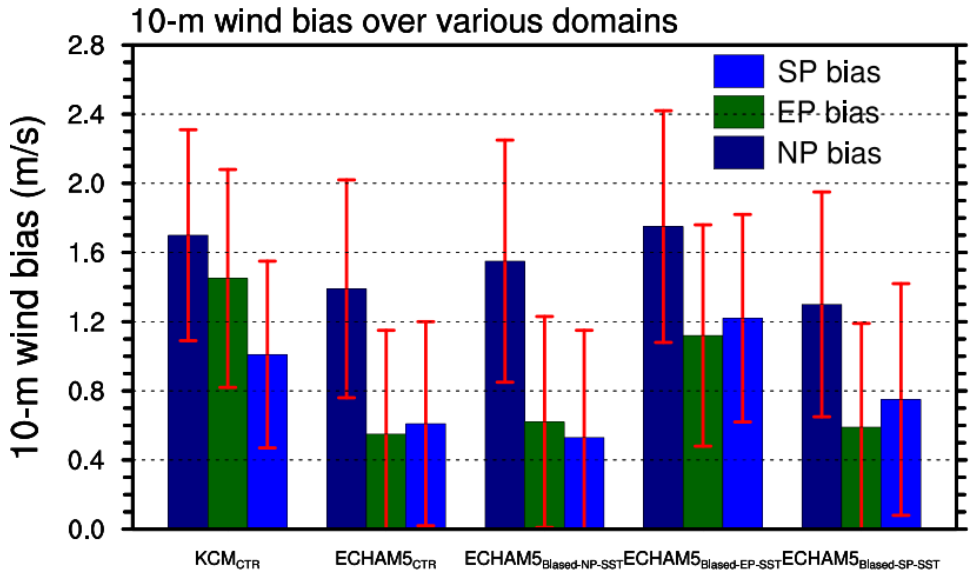

Figure 12. 10-m wind bias over different domains in KCM$_{CTR}$ and the stand-alone

Accepted for publication in *Journal of Climate*. DOI 10.1175/JCLI-D-22-0874.1.

atmospheric experiments with respect to the NCEP/CFSR reanalysis averaged over the period of 1982-2017. Red error bars indicate the uncertainty of 10-m wind biases, defined as one standard deviation of monthly wind biases.

We can infer from the uncoupled AGCM experiments that significant 10-m wind-speed biases are already present in the atmosphere model, and that they are amplified and expanded in the coupled mode with large differences between the three regions. Over the NP most of the wind bias in the KCM_{CTR} is due to the atmosphere model, and this bias is slightly amplified in the coupled mode mainly due to the SST biases in the NP and EP (increase by 20% from 1.39 m/s in $ECHAM5_{CTR}$ to 1.70 m/s in KCM_{CTR}). Over the eastern subtropical SP, the wind bias is also mainly due to the atmosphere model, but the amplification over the central and eastern SP by coupling is larger than over the NP, mainly caused by the SST biases in the SP and EP (increase by 64% from 0.61 m/s in $ECHAM5_{CTR}$ to 1.01 m/s in KCM_{CTR}). Over the EP, the local coupling is the largest contributor to the wind bias (increase by 160% from 0.55 m/s in $ECHAM5_{CTR}$ to 1.45 m/s in KCM_{CTR}).

4 Summary and discussion

A control integration of the KCM (KCM_{CTR}), as many CMIP5 and CMIP6 models, exhibits pronounced cold SST biases over the northern tropical Pacific (NP), equatorial Pacific (EP) and southern tropical Pacific (SP). Over these regions, the models also suffer from strong easterly surface-wind biases. In the CMIP5 and CMIP6 historical simulations, we find that the SST bias is strongly related to the easterly wind strength over the EP. Furthermore, the zonal surface-wind strength over the EP is correlated with those over the NP and SP.

The origin of biases in SST over the Pacific and their relationship to the near-surface (10-m) winds is investigated by means of dedicated experiments with the KCM and stand-alone experiments with its atmospheric component. When the NCEP/CFSR reanalysis-wind stress is specified globally in the coupled model, the cold SST bias over the EP is completely reduced relative to the KCM_{CTR}. Additional coupled sensitivity

Accepted for publication in *Journal of Climate.* DOI 10.1175/JCLI-D-22-0874.1.

experiments are conducted to investigate the influence of the surface-wind biases over selected regions on the cold SST bias over the EP. The excessively strong easterlies over the EP are the major contributor to the cold SST bias over the EP, with the wind biases over the NP and SP having a much smaller influence, which, however, cannot be ignored. When reanalysis-wind stress is specified over the EP, the cold SST bias there is alleviated by 52%, when specified over the NP by 12%, and when specified over the SP by 23%.

In the KCM_{CTR}, the cold SST bias over the EP is dominated by dynamical cooling due to too strong zonal westward and meridional poleward currents, and too strong upwelling. The sensitivity experiments with the KCM show that reanalysis-wind stress when only specified over the EP weakens the local equatorial currents, thereby reducing considerably the cold SST bias over the region. Therefore, the influence of processes in the vertical direction is much weaker compared to the horizontal processes. Reanalysis-wind stress specified over the NP and SP also alleviates the cold SST bias over the EP but to a much lesser extent. Analysis of surface-heat flux and cloud cover reveals that in contrast to the dynamical coupling by winds the thermodynamic coupling counteracts the cold SST bias over the EP.

The origin of the overly strong easterly wind stress in the three selected regions is investigated by a set of stand-alone experiments with the ECHAM5, the atmospheric component of the KCM. The results suggest that the atmosphere model by itself simulates a large wind bias over the NP and smaller biases over the EP and SP, which amount to 82%, 38% and 60% of those in the KCM_{CTR}, respectively. The cold SST bias over the EP substantially enhances the wind biases over all three considered regions, while the SST biases over the NP and SP regions mainly support local amplification of the wind bias. Thus, the cold SST bias over the EP is mainly due to the (coupled) Bjerknes feedback and further enhanced by too cold subtropical SSTs. Previous studies identified two pathways for subtropical SSTs to influencing equatorial SST: one major pathway, reaching down to a depth of about 600 m, which follows the recirculation near the western boundary of the Pacific basin and then shoals towards the equator and Equatorial Undercurrent. The other connects the equator with off-equatorial regions

Accepted for publication in *Journal of Climate.* DOI 10.1175/JCLI-D-22-0874.1.

through the shallow overturning cells in the central and eastern Pacific (Gu and Philander, 1997; Thomas and Fedorov, 2017; Burls et al., 2017).

It is noted that the experiments EP-Wind, NP-Wind and SP-Wind together explain 87% of the SST bias over the EP assuming linearity of the response, which is 13% less relative to the Global-Wind. The contributions from other tropical basins, i.e., the tropical Atlantic and the tropical Indian Ocean, may also be important to the cold bias over the EP (Cvijanovic and Chiang, 2013; Meehl et al., 2021). As many CMIP models, the KCM_{CTR} suffers from a weaker Atlantic Meridional Overturning Circulation (AMOC, Wang et al., 2014) relative to present-day estimates that could lead to a cold SST bias over the northern tropical Atlantic. In the ECHAM5 atmosphere model, local cold SST biases contribute to overly strong surface winds over the northern tropical Atlantic that is as part of a westward shift of the Walker circulation (Svendsen et al., 2014), which in turn could influence surface winds and SST over the EP. Pacemaker experiments that assimilate warming SST trend over the Indian Ocean favourably yields cooling SST trends of the equatorial Pacific via the Walker Circulation (Mochizuki et al., 2016). Remote forcing from the Atlantic and the Indian Ocean, however, appears not to play a crucial role in the KCM, as most of the SST biases over the tropical Pacific can be explained by local processes.

Large uncertainties in the observational surface heat fluxes, especially over the off-equatorial region and over the eastern equatorial Pacific, limit the assessment for the responses of surface heat fluxes to the SST biases. The changes of surface heat fluxes in the sensitivity experiment are comparable to the observational uncertainty (Figure 9). Similarly, the response of surface winds to the biased SSTs as simulated in the stand-alone atmosphere-model experiments are weaker than the uncertainties in the NCEP/CFSR reanalysis (Figure 12). The reasons are twofold. First, large uncertainties exist in the NCEP/CFSR surface winds. Second, we evaluate the wind biases in the coupled and stand-alone atmosphere-model experiments using the same definition of the EP, NP and SP regions. Yet the bias pattern in the coupled experiment differs from the atmosphere-only experiment (Figure 1 and Figure 11).

In this study, we use the wind stress from the NCEP/CFSR reanalysis as a forcing

Accepted for publication in *Journal of Climate.* DOI 10.1175/JCLI-D-22-0874.1.

in partially coupled experiments. We note that ocean-sea ice models can be quite sensitive to the atmospheric forcing dataset, which causes significant differences in the simulated ocean circulation (e.g., Hunke and Holland, 2007; Lindsay et al. 2014). Thus, our results may be dependent on the applied wind stresses. On the other hand, the intercomparison of atmospheric reanalysis products shows that they are comparable due to similar physical assumptions and assimilation of common observations (Chaudhuri et al., 2013; Stopa and Cheung, 2014). Therefore, a different choice of the atmospheric forcing dataset may not necessarily change the main conclusion of this study that the SST bias over the EP is linked to the equatorial and subtropical surface-wind biases, both of which being amplified through ocean-atmosphere interaction. This hypothesis is supported by another set of partially coupled experiments with the KCM forced by the ERA-Interim wind stresses (Figure S11). EP SST biases in the simulations forced by the ERA-interim winds are similar yet relatively larger than those forced by the NCEP/CFSR winds.

Suffering from limitations such as a constant MLD in the heat budget analysis and relatively different wind bias pattern in the KCM, our results still provide implications for improving some CGCMs. As indicated by our stand-alone atmosphere model experiments, the surface-wind biases are largely internal to the atmosphere model with the patterns and intensities of biases being influenced by coupling especially over the EP. This is consistent with the study of Harlaß et al. (2017), who investigated the warm tropical Atlantic SST bias. Thus, one way to reduce tropical SST biases in CGCMs is to improve the atmospheric components. Roberts et al. (2009) reported that increasing the horizontal resolution in the atmosphere model improves simulation of surface winds and SST in the Hadley Centre Global Environmental Model version 1. Jung et al. (2012) suggested that shorter time steps rather than increased horizontal resolution in the atmosphere model helps to improve the near-surface winds over the tropical Pacific as well as the mean meridional atmospheric circulation in the tropics. This study also implies that improving the surface winds in the atmosphere model holds a large potential to enhance the simulation of tropical Pacific mean climate in CGCMs.

Accepted for publication in *Journal of Climate.* DOI 10.1175/JCLI-D-22-0874.1.

Acknowledgments

The suggestions of the three anonymous referees greatly improved an earlier version of the manuscript. The integration with the Kiel Climate Model (KCM) was conducted at the Computing Centre of Kiel University (CAU). We thank Joakim Kjellsson for his helpful comments and discussions. ZS is supported by the National Natural Science Foundation of China (Grant No. 42206206) and Natural Science Foundation of Guangdong province (Grant No. 2022A1515010917). YZ is sponsored by the China Scholarship Council (CSC) and supported by the Fundamental Research Funds for the Central Public Welfare Scientific Institutes (Grant No. PM-zx703-202104-091). TB is supported by the Deutsche Forschungsgemeinschaft (DFG) project "Influence of Model Bias on ENSO Projections of the 21st Century" through grant 429334714 and AR by the European Union's Horizon 2020 research and innovation programme under the Marie Skłodowska-Curie grant agreement No. 101026271.

Data Availability Statement

CMIP data were retrieved from the Earth System Grid Federation (https:// esgf-node.llnl.gov/projects/cmip6/) and the KCM output is archived at the Zenodo repository (https://zenodo.org/deposit/7376944#). Observational datasets required for the analysis are available freely at the locations cited in the text.

References

Alexander MA, Bladé I, Newman M et al (2002). The atmospheric bridge: the influence of ENSO teleconnections on air–sea interaction over the global oceans. *J. Clim.,* 15:2205–2231. Doi:10.1175/1520-0442(2002)015<2205:TABTIO>2.0.CO;2.

Bayr T, Latif M, D., Dommenget, C., Wengel, J., Harlaß and W., Park (2018). Mean-state dependence of ENSO atmospheric feedbacks in climate models. Clim Dyn 50:3171–3194. https:// doi. org/ 10. 1007/ s00382- 017- 3799-2

Bayr T, Wengel C, Latif M, Dommenget D, Lübbecke J, and Park W (2019a). Error compensation of ENSO atmospheric feedbacks in climate models and its influence on simulated ENSO dynamics, Climate Dynamics 53:155–172. Doi:10.1007/s00382-018-4575-7.

Bayr T, Dommenget D, Latif M (2020) Walker circulation controls ENSO atmospheric feedbacks in uncoupled and coupled climate model simulations. Clim Dyn 54:2831–2846. https://doi.org/10.1007/s00382-020-05152-2.

Bayr T, D., Domeisen, Wengel C (2019b). The effect of the equatorial Pacific cold SST bias on simulated ENSO teleconnections to the North Pacific and California Climate Dynamics:19. Doi:10.1007/s00382-019-04746-9.

Bayr, T., Drews, A., Latif, M and J., Lübbecke (2021). The interplay of thermodynamics and ocean dynamics during ENSO growth phase. Clim Dyn 56, 1681–1697 https://doi.org/10.1007/s00382-020-05552-4.

Bellenger H, Guilyardi E, Leloup J, Lengaigne M, Vialard J (2014). ENSO representation in climate models: from CMIP3 to CMIP5. Climate Dynamics 42:1999-2018.

Beobide-Arsuaga G, Bayr T, Reintges A, Latif M (2021) Uncertainty of ENSO-amplitude projections in CMIP5 and CMIP6 models. Clim Dyn 56:3875–3888. https://doi.org/10.1007/s00382-021-05673-4.

Boyer, Tim P.; Garcia, Hernan E.; Locarnini, Ricardo A.; Zweng, Melissa M.; Mishonov, Alexey V.; Reagan, James R.; Weathers, Katharine A.; Baranova, Olga K.; Seidov, Dan; Smolyar, Igor V. (2018). World Ocean Atlas 2018. NOAA National Centers for Environmental Information. Dataset. https://www.ncei.noaa.gov/archive/accession/NCEI-WOA18.

Burls NJ, Muir L, Vincent EM, Fedorov A (2017). Extra-tropical origin of equatorial Pacific cold bias in climate models with links to cloud albedo. Climate Dynamics 49:2093-2113.

Cai W, Santoso A, Collins M, et al (2021) Changing El Niño–Southern Oscillation in a warming climate. Nat Rev Earth Environ 0123456789: https://doi.org/10.1038/s43017-021-00199-z.

Chaudhuri AH, Ponte RM, Forget G, Heimbach P (2013). A Comparison of Atmospheric Reanalysis Surface Products over the Ocean and Implications for Uncertainties in Air–Sea Boundary Forcing Journal of Climate 26:153-170. Doi:10.1175/jcli-d-12-00090.1.

Chiang JCH, Bitz CM (2005). Influence of high latitude ice cover on the marine intertropical convergence zone. Clim Dyn 25:477– 496. doi:10.1007/s00382-005-0040-5.

Cvijanovic I, Chiang JCH (2013). Global energy budget changes to high latitude North Atlantic cooling and the tropical ITCZ response. Clim Dyn 40:1435–1452. doi:10.1007/ s00382-012-1482-1.

Davey M, Huddleston M, Sperber K, et al (2002) STOIC: A study of coupled model climatology and variability in tropical ocean regions. Clim Dyn 18:403–420. https://doi.org/10.1007/s00382-001-0188-6.

Dee, D. P., Uppala, S. M., Simmons, A. J., Berrisford, P., Poli, P., Kobayashi, S., et al. (2011). The ERA□interim reanalysis: Configuration and performance of the data assimilation system. Quarterly Journal ofthe Royal Meteorological Society, 137(656), 553–597. https://doi.org/ 10.1002/qj.828.

Ding, H., M. Newman, M. A. Alexander, and A. T. Wittenberg (2020). Relating CMIP5 model biases to seasonal forecast skill in the tropical Pacific. Geophys. Res. Lett., 47, doi: 10.1029/2019GL086765.

DiNezio PN, Clement AC, Vecchi GA, Soden BJ, Kirtman BP, Lee S-K (2009). Climate Response of the Equatorial Pacific to Global Warming. Journal of Climate 22:4873-4892.

Eyring, V., Bony, S., Meehl, G. A., Senior, C. A., Stevens, B., Stouffer, R. J., & Taylor, K. E. (2016). Overview of the Coupled Model Intercomparison Project Phase 6 (CMIP6) experimental design and organization. Geoscientific Model Development, 9(5), 1937–1958. https://doi.org/10.5194/gmd-9-1937-2016.

Ferrett, S., Collins, M., & Ren, H. (2018). Diagnosing Relationships between Mean State Biases and El Niño Shortwave Feedback in CMIP5 Models, Journal of Climate, 31(4), 1315-1335. https://doi.org/10.1175/JCLI-D-17-0331.1.

Gordon CT, Rosati A, Gudgel R (2000). Tropical sensitivity of a cou- pled model to specified ISCCP low clouds. J Clim 13:2239– 2260. Doi:10.1175/1520-0442(2000)013<2239:TSOACM>2.0 . CO;2.

Gu D., and S G. H. Philander (1997), Interdecadal Climate Fluctuations That Depend on Exchanges Between the Tropics and Extratropics. Science 275, 805-807. DOI:10.1126/science.275.5301.805.

Guilyardi E, Wittenberg AT, Fedorov A, et al (2009) Understanding El Nino in Ocean–Atmosphere General Circulation Models: Progress and Challenges. Bull Am Meteorol Soc 90:325–340. https://doi.org/10.1175/2008BAMS2387.1.

Guilyardi E, Braconnot P, Jin F-F et al (2010). Atmosphere feedbacks during ENSO in a coupled GCM with a modifed atmospheric convection scheme. J Clim 22:5698–5718.

Doi:10.1175/2009JCLI2815.1.

Guilyardi E, Capotondi A, Lengaigne M, et al (2020) Chapter 9: ENSO Modeling: History, Progress, and Challenges. In: El Niño Southern Oscillation in a Changing Climate. pp 201–226.

Harlaß, J., M. Latif, and W. Park (2017). Alleviating Tropical Atlantic Sector Biases in the Kiel Climate Model by Enhancing Horizontal and Vertical Atmosphere Model Resolution: Climatology and Interannual Variability. Climate Dynamics, doi:10.1007/s00382-017-3760-4.

He J, Johnson NC, Vecchi GA et al (2018) Precipitation sensitivity to local variations in tropical sea surface temperature. J Clim 31:9225–9238. https:// doi. org/ 10. 1175/ JCLI-D- 18- 0262.1.

He Z, Wu R, Wang W, Wen Z, Wang D (2017). Contributions of Surface Heat Fluxes and Oceanic Processes to Tropical SST Changes: Seasonal and Regional Dependence. Journal of Climate 30:4185-4205.

Hersbach, H., de Rosnay, P., Bell, B., Schepers, D., Simmons, A., Soci, C., et al. (2018). Operational global reanalysis: Progress, future directions and synergies with NWP. ERA Report Series. doi: https://doi.org/10.21957/tkic6g3wm.

Hunke EC, Holland MM (2007). Global atmospheric forcing data for Arctic ice-ocean modeling. Journal of Geophysical Research 112.

Izumo T, Vialard J, Lengaigne M, Suresh I (2019) Relevance of relative sea surface temperature for tropical rainfall interannual variability. Geophys Res Lett. https:// doi. org/ 10. 1029/ 2019g l0861 82.

Jung T et al. (2012). High-Resolution Global Climate Simulations with the ECMWF Model in Project Athena: Experimental Design, Model Climate, and Seasonal Forecast Skill Journal of Climate 25:3155-3172. Doi:10.1175/jcli-d-11-00265.1.

Klein SA, J. SB, Lau N-C (1999). Remote sea surface temperature variations during ENSO: evidence for a tropical atmospheric bridge. Journal of Climate 12:917-932.

Li G, Xie S-P (2014). Tropical biases in CMIP5 multimodel ensemble: the excessive equatorial Pacific cold tongue and double ITCZ problems. J Clim 27:1765–1780. Doi:10.1175/JCLI-D-13-00337.1.

Lin J-L (2007). The double-ITCZ problem in IPCC AR4 coupled GCMs: ocean-atmosphere feedback analysis. J Clim 20:4497–4525. Doi:10.1175/JCLI4272.1.

Lindsay R, Wensnahan M, Schweiger A, Zhang J (2014). Evaluation of seven different atmospheric

reanalysis products in the Arctic. Journal of Climate 27:2588-2606.

Liu Z, Yang H (2003). Extratropical control of tropical climate, the atmospheric bridge and oceanic tunnel. Geophysical Research Letters 30:1230.

Lloyd J, Guilyardi E, Weller H, Slingo J (2009) The role of atmosphere feedbacks during ENSO in the CMIP3 models. Atmos Sci Lett 10:170–176. https://doi.org/10.1002/asl.227.

Madec G (2008). NEMO ocean engine. Note du Pole modélisation 27, Inst. Pierre-Simon Laplace, p 193

Mauritsen, T., B., Stevens, E., Roeckner, T., Crueger, M., Esch, M., Giorgetta, H., Haak, J., Jungclaus, D., Klocke, D., Matei, U., Mikolajewicz, D., Notz, R., Pincus, H., Schmidt and L., Tomassini (2012). Tuning the climate of a global model, J. Adv. Model. Earth Syst., 4, M00A01, doi:10.1029/2012MS000154.

McCreary JP Jr, Lu P (1994). Interaction between the subtropical and equatorial ocean circulations: the subtropical cell. Journal of Physical Oceanography 24:466-497

Mechoso CR, Robertson AW, Barth N et al (1995). The Seasonal cycle over the tropical pacific in coupled ocean–atmosphere general circulation models. Mon Weather Rev 123:2825–2838.

Meehl, G.A., Hu, A., Castruccio, F. et al. Atlantic and Pacific tropics connected by mutually interactive decadal-timescale processes. Nat. Geosci. 14, 36–42 (2021). https://doi.org/10.1038/s41561-020-00669-x.

Mochizuki, T., Kimoto, M., Watanabe, M., Chikamoto, Y., and Ishii, M. (2016), Interbasin effects of the Indian Ocean on Pacific decadal climate change, Geophys. Res. Lett., 43, 7168– 7175, doi:10.1002/2016GL069940.

Moum JN, Perlin A, Nash JD, McPhaden MJ (2013). Seasonal Sea sur- face cooling in the equatorial Pacific cold tongue controlled by ocean mixing. Nature 500:64–67. Doi:10.1038/nature12363.

Murtugudde, R., J. Beauchamp, C. R. McClain, M. Lewis, and A. J. Busalacchi (2002). Effects of penetrative radiation on the upper tropical ocean circulation. J. Climate, 15, 470–486, doi:10.1175/1520-0442(2002)015<0470:EOPROT>2.0.CO;2.

Park W, Keenlyside N, Latif M, Ströh A, Redler R, Roeckner E, Madec G (2009). Tropical Pacific climate and its response to global warming in the Kiel Climate model. J Clim 22(1):71–92.

Planton YY, Guilyardi E, Wittenberg AT, et al (2021). Evaluating climate models with the CLIVAR 2020 ENSO metrics package. Bull Am Meteorol Soc 102:E193–E217.

Accepted for publication in *Journal of Climate.* DOI 10.1175/JCLI-D-22-0874.1.

https://doi.org/10.1175/BAMS-D-19-0337.1.

Rayner NA, Parker DE, Horton EB, Folland CK, Alexander L V, Rpwell D P, Kent E C, Kaplan A (2003). Global analyses of sea surface temperature, sea ice, and night marine air temperature since the late nineteenth century. Journal of Geophysical Research 108

Richards, K. J., Xie, S., & Miyama, T. (2009). Vertical Mixing in the Ocean and Its Impact on the Coupled Ocean–Atmosphere System in the Eastern Tropical Pacific, Journal of Climate, 22(13), 3703-3719. https://doi.org/10.1175/2009JCLI2702.1.

Roberts MJ, Clayton A, Demory M-E, et al (2009). Impact of Resolution on the Tropical Pacific Circulation in a Matrix of Coupled Models. Journal of Climate 22(10): 2541-2556. Doi: https://doi.org/10.1175/2008JCLI2537.1

Roeckner E, Bäuml G, Bonaventura L et al (2003). The atmospheric general circulation model ECHAM5. PART I: model description, Report 349. Max Planck Institute for Meteorology, Hamburg, p 140

Saha S, Moorthi S, Pan H-L, et al (2010). The NCEP Climate Forecast System Reanalysis. Bulletin of the American Meteorological Society 91:1015-1058

Seager R, Cane M, Henderson N, et al (2019) Strengthening tropical Pacific zonal sea surface temperature gradient consistent with rising greenhouse gases. Nat Clim Chang 9:517–522. https://doi.org/10.1038/s41558-019-0505-x.

Seager R, Henderson N, Cane M (2022) Persistent discrepancies between observed and modeled trends in the tropical Pacific Ocean. J Clim 1–41. https://doi.org/10.1175/jcli-d-21-0648.1.

Simmons A, Uppala S, Dee D, Kobayashi S (2007). ERA-Interim: new ECMWF reanalysis products from 1989 onwards. ECMWF Newsl 110:25–35

Small, R. J., J., Bacmeister, D., Bailey, A., Baker, S., Bishop, F., Bryan, J., Caron, J., Dennis, P., Gent, H., Hsu, M., Jochum, D., Lawrence, E., Muñoz, P., DiNezio, T., Scheitlin, R., Tomas, J., Tribbia, Y., Tseng, and M., Vertenstein (2014). A new synoptic scale resolving global climate simulation using the Community Earth System Model, J. Adv. Model. Earth Syst., 6, 1065–1094, doi:10.1002/2014MS000363.

Song X, Zhang GJ (2009). Convection Parameterization, Tropical Pacific Double ITCZ, and Upper-Ocean Biases in the NCAR CCSM3. Part I: Climatology and Atmospheric Feedback. Journal

of Climate 22:4299-4315

Stopa JE, Cheung KF (2014). Intercomparison of wind and wave data from the ECMWF Reanalysis Interim and the NCEP Climate Forecast System Reanalysis Ocean Modelling 75:65-83. Doi:10.1016/j.ocemod.2013.12.006.

Sun D-Z, Fasullo J, Zhang T, Roubicek A (2003). On the radiatie and dynamical feedbacks over the equatorial Pacific cold tongue. Journal of Climate 16:2425-2432.

Svendsen, L., Kvamstø, N.G. & N., Keenlyside (2014). Weakening AMOC connects Equatorial Atlantic and Pacific interannual variability. Clim Dyn 43, 2931–2941 https://doi.org/10.1007/s00382-013-1904-8.

Taylor KE, Stouffer RJ, Meehl GA (2012). An overview of CMIP5 and the experiment design. Bull Am Meteorol Soc 93:485–498. Doi:10.1175/BAMS-D-11-00094.1.

Thomas, M. D., & Fedorov, A. V. (2017). The Eastern Subtropical Pacific Origin of the Equatorial Cold Bias in Climate Models: A Lagrangian Perspective, Journal of Climate, 30(15), 5885-5900. https://doi.org/10.1175/JCLI-D-16-0819.1.

Timmermann A et al (2018). El Niño-Southern Oscillation Complexity Nature 559:535-545. Doi:10.1038/s41586-018-0252-6

Vannière B, Guilyardi E, Madec G, Doblas-Reyes FJ, Woolnough S (2013). Using seasonal hindcasts to understand the origin of the equatorial cold tongue bias in CGCMs and its impact on ENSO. Climate Dynamics 40:963-981.

Vannière B, Guilyardi E, Toniazzo T, Madec G, Woolnough S (2014). A systematic approach to identify the sources of tropical SST errors in coupled models using the adjustment of initialized experiments. Climate Dynamics 43:2261-2282.

Wang C, Zhang L, Lee S-K, Wu L, Mechoso CR (2014). A global perspective on CMIP5 climate model biases. Nature Climate Change 4:201-205.

Wengel C, Latif M, Park W, Harlaß J, Bayr T (2018). Seasonal ENSO phase locking in the Kiel Climate Model: The importance of the equatorial cold sea surface temperature bias. Climate Dynamics 50:901-919.

Yeh S-W, Cai W, Min S-K, et al (2018). ENSO Atmospheric Teleconnections and Their Response to Greenhouse Gas Forcing. Reviews of Geophysics 56(1):185-206. Doi: https://doi.org/10.1002/2017RG000568.

Accepted for publication in *Journal of Climate.* DOI 10.1175/JCLI-D-22-0874.1.

Yu, L., X. Jin, and R. A. Weller (2008). Multidecade global flux datasets from the objectively analyzed air–sea fluxes (OAFlux) project: latent and sensible heat fluxes, ocean evaporation, and related sur- face meteorological variables. OAFlux project technical report. OA-2008-01, 64pp.

Zhang, Y., and W.B. Rossow (2023). Global radiative flux profile data set: Revised and extended. Journal of Geophysical Research: Atmospheres, 128, e2022JD037340. https://doi.org/10.1029/2022JD037340.

Zhang GJ, Song X (2010). Convection parameterization, tropical Pacific double ITCZ, and upper-ocean Biases in the NCAR CCSM3. Part II: coupled feedback and the role of ocean heat transport Journal of Climate 23:800-812. Doi:10.1175/2009jcli3109.1

Accepted for publication in *Journal of Climate.* DOI 10.1175/JCLI-D-22-0874.1.